Type III Collagen is a Key Regulator of the Collagen Fibrillar Structure and Biomechanics of Articular Cartilage and Meniscus

Chao Wang,[1] Becky K. Brisson,[2] Masahiko Terajima,[3] Qing Li,[1] Kevt'her Hoxha,[1] Biao Han,[1] Abby M. Goldberg,[2] X. Sherry Liu,[4] Michele S. Marcolongo,[5] Motomi Enomoto-Iwamoto,[6] Mitsuo Yamauchi,[3] Susan W. Volk,[2,] Lin Han[1,*]*

[1]*School of Biomedical Engineering, Science and Health Systems, Drexel University, Philadelphia, PA 19104, United States*

[2]*Department of Clinical Sciences and Advanced Medicine, University of Pennsylvania, School of Veterinary Medicine, Philadelphia, PA 19104, United States*

[3]*NC Oral Health Institute, University of North Carolina, Chapel Hill, NC 27599, United States*

[4]*McKay Orthopaedic Research Laboratory, Department of Orthopaedic Surgery, Perelman School of Medicine, University of Pennsylvania, Philadelphia, PA 19104, United States*

[5]*Department of Materials Science and Engineering, Drexel University, Philadelphia, PA 19104, United States*

[6]*Department of Orthopaedics, School of Medicine, University of Maryland, Baltimore, MD 21201, United States*

*Correspondence and requests for materials should be addressed to:

Dr. Lin Han, Phone: (215)571-3821, Fax: (215)895-4983, Email: lh535@drexel.edu.

Dr. Susan W. Volk, Phone: (215)895-0635, Fax: (215)573-6050, Email: swvolk@vet.upenn.edu.

For submission to *Matrix Biology* as a *Full Length Article.*

Abstract

Despite the fact that type III collagen is the second most abundant collagen type in the body, its contribution to the physiologic maintenance and repair of skeletal tissues remains poorly understood. This study queried the role of type III collagen in the structure and biomechanical functions of two structurally distinctive tissues in the knee joint, type II collagen-rich articular cartilage and type I collagen-dominated meniscus. Integrating outcomes from atomic force microscopy-based nanomechanical tests, collagen fibril nanostructural analysis, collagen cross-linking analysis and histology, we elucidated the impact of type III collagen haplodeficiency on the morphology, nanostructure and biomechanical properties of articular cartilage and meniscus in *Col3a1*$^{+/-}$ mice. Reduction of type III collagen leads to increased heterogeneity and mean thickness of collagen fibril diameter, as well as reduced modulus in both tissues, and these effects became more pronounced with skeletal maturation. These data suggest a crucial role of type III collagen in mediating fibril assembly and biomechanical functions of both articular cartilage and meniscus during post-natal growth. In articular cartilage, type III collagen has a marked contribution to the micromechanics of the pericellular matrix, indicating a potential role in mediating the early stage of type II collagen fibrillogenesis and chondrocyte mechanotransduction. In both tissues, reduction of type III collagen leads to increased collagen cross-linking despite the decrease in modulus. This suggests that the disruption of matrix structure due to type III collagen deficiency outweighs the stiffening of collagen fibrils by increased cross-linking, leading to a net negative impact on tissue modulus. Collectively, this study is the first to highlight the crucial structural role of type III collagen in both articular cartilage and meniscus extracellular matrices. We expect these results to expand our understanding of type III collagen across various tissue types, and to uncover critical molecular components of the microniche for regenerative strategies targeting articular cartilage and meniscus repair.

Keywords: Type III collagen, collagen fibrils, aggrecan, pericellular matrix, atomic force microscopy.

1. Introduction

Type III collagen (collagen III) is the second most abundant collagen type in human body [1], and a crucial structural constituent of fibrillar collagen organization. Collagen III frequently co-assembles with collagen I to form heterotypic type I/III fibrils in many collagen I-dominant fibrous tissues [2], and has been attributed to controlling fibril diameter and involving in collagen cross-linking [3, 4]. A major role of collagen III in human health is supported by phenotypes of individuals who possess an autosomal dominant mutation of the human *COL3A1* gene. These vascular Ehlers-Danlos Syndrome (vEDS) patients are at increased lethal risk of vascular and organ rupture, and exhibit signs associated with premature aging as well as degeneration of musculoskeletal tissues [5-7]. Similarly, haplodeficiency of collagen III in mice (*Col3a1*$^{+/-}$) leads to the development of vascular lesions reminiscent of human lesions [8] and diminished quality of cutaneous wound repair during aging [9]. In the *Col3a1*$^{+/-}$ model, reduction of collagen III also shows marked impacts on neocortical development [10, 11], development and repair of the skeleton [12, 13], and tumor microenvironment [14]. Homozygous ablation of collagen III in mice (*Col3a1*$^{-/-}$) results in a low survival rate (< 3.5%) to weaning, with the few surviving adults succumbing to catastrophic failure of vascular and intestinal tissues [4]. Despite long-standing recognition of collagen III's importance in tissue development, maintenance and repair, the contribution of collagen III to the matrix collagen fibril structure and biomechanical properties of tissue remain poorly defined [15]. While collagen III has been shown to frequently co-exist with collagen I [4, 16, 17], previous studies also suggest that it interacts with collagen II [18, 19], the major collagen type in hyaline cartilage. However, whether it plays a role as a crucial structural constituent of cartilage is unknown.

In this study, we queried the contribution of collagen III to the structure and biomechanics of knee articular cartilage. Meanwhile, to compare the activities of collagen III in tissues consisting of collagen I versus those of collagen II, we also studied the meniscus, a collagen I-dominated fibrocartilage. In the knee joint, the two tissues work in concert to enable everyday activities. Articular cartilage provides compressive load bearing [20], shock absorption through poroviscoelastic energy dissipation [21] and lubrication [22]. These functions are endowed by its specialized extracellular matrix (ECM) consisting of collagen II/IX/XI fibrillar network

entrapping the highly negatively charged proteoglycan, aggrecan [23]. Meniscus mainly sustains the tensile "hoop" stress to provide joint stability and facilitate load transmission and redistribution [24]. The meniscal ECM consists of circumferentially oriented collagen I fiber bundles wrapped in radially oriented superficial layer and radial tie fibers, with much lower proteoglycan content [25-27]. Despite the distinct structure and mechanical functions of the two tissues, collagen III is present in both [19, 28, 29]. In human articular cartilage, collagen III content increases in the territorial matrix of aging individuals, although it remains unclear whether this increase represents a protective response to cartilage degeneration or a contributor to the pathological process [30]. While the overall collagen III content (~ 1-5% of total) is low compared to other ECM components in articular cartilage, its concentrated distribution surrounding the cellular microenvironment suggests that collagen III could play a profound role in regulating cell activities. In addition, unlike collagen II fibrils, collagen III undergoes highly dynamic metabolic turnover in vivo, as evidenced by the high concentration of collagen III N-propeptides in urine [31]. The content of collagen III thus could vary markedly at different stages of development and disease. In human OA, collagen III is significantly up-regulated in cartilage [30] and its degradation neo-epitopes could potentially serve as a biomarker of cartilage degeneration [32]. In healthy meniscus, collagen III is expressed throughout the tissue although more concentrated along the exterior peripheral border, on the surface, and in the vessels of the outer zone. In degenerative meniscus, collagen III content decreases proportionately to the degree of degradation [33]. Determination of the role of collagen III in regulating the matrix structure and biomechanical functions of these tissues would have tremendous implications for the development of preventative and therapeutic strategies to improve the health of articular cartilage and meniscus [34, 35].

The objective of this study was to determine if collagen III is a key constituent in the structural integrity and biomechanical functions of articular cartilage and meniscus. To achieve this goal, using *Col3a1*$^{+/-}$ mice, we studied the impact of collagen III reduction on the structure and biomechanical properties of both tissues. Applying electron microscopy, we measured the nanostructure of collagen fibrils on tissue surfaces and in the matrix interior. Applying our recently established AFM nanomechanical tests [36-39], we evaluated the impact

of collagen III reduction on the biomechanical properties of both tissues. In cartilage, the pericellular matrix (PCM) has distinct composition and structure from the territorial/interterritorial domains (T/IT-ECM) that are further-removed from cells [40, 41], and collagen III is preferentially distributed in the PCM [30, 42]. We thus also studied the role of collagen III in the micromechanics of cartilage PCM. Further, since collagen III actively participates in cartilage collagen cross-linking [19], we analyzed the changes in collagen cross-links upon collagen III reduction. Outcomes showed that the reduction of collagen III leads to substantial alteration of collagen fibril architecture, cross-linking as well as biomechanical properties of both tissues. These evidences highlighted collagen III as an indispensable matrix constituent in both collagen II-rich articular cartilage and collagen I-dominated meniscus.

2. Results

2.1 Reduction of collagen III does not result in gross-level phenotype in articular cartilage.

In *Col3a1*$^{+/-}$ mice, the expression of *Col3a1* was reduced in both cartilage and meniscus by ≈ 50% in comparison to the wild-type (WT) control, while other major matrix genes were not significantly altered, as shown by qPCR (Fig. 1a, $n = 4$ biological repeats for WT control, $n = 3$ for *Col3a1*$^{+/-}$). We then investigated the presence and distribution of collagen III via immunohistochemistry (IHC). At 2-week age, we did not detect a clear distribution pattern of collagen III throughout the matrix (Fig. 1b). At 2-month age, collagen III became more concentrated in the PCM (Fig. 1b), similar to that of healthy adult human cartilage [30, 42]. At the protein level, *Col3a1*$^{+/-}$ cartilage showed reduced immunostaining of collagen III, but retained its spatial distribution (Fig. 1b). Here, we validated the specificity of collagen III antibody by western blot analysis on recombinant human collagen I and III, as well as collagen II extracted from human cartilage (Fig. 1c). Despite the reduction of collagen III, *Col3a1*$^{+/-}$ mice did not show noticeable gross defects in cartilage, as signified by similar histological staining of sulfated glycosaminoglycans (sGAGs) (Fig. 1d), cartilage thickness and total amount of sGAGs (Fig. 1e).

2.2 Reduction of collagen III leads to reduced modulus of cartilage and meniscus.

In young adult mice, despite a lack of obvious histological phenotype of the knee joint, both articular cartilage and meniscus showed significantly lower moduli associated with the reduction in collagen III (Fig. 2). In 2-month-old mice, the modulus of cartilage in *Col3a1*$^{+/-}$ mice (0.9 ± 0.6 MPa, mean ± 95% CI, $n = 7$) was lower than WT (2.3 ± 0.6 MPa, $n = 7$) by 59 ± 4 % ($p = 0.011$, Fig. 2a). Since cartilage modulus is directly governed by two major ECM constituents, the aggrecan aggregates and collagen fibrillar network [43], we delineated the impact of collagen III deficiency on each constituent by testing the tissue after enzymatic removal of the sGAGs on aggrecan. The removal of sGAGs, as expected, significantly reduced cartilage moduli in both genotypes. Further, after sGAG removal, the modulus of *Col3a1*$^{+/-}$ cartilage (0.2 ± 0.1 MPa, $n = 5$), which is now dominated by the collagen fibrillar network, remained to be lower than that of the WT (0.7 ± 0.2 MPa, $n = 6$) by 72 ± 7 % ($p < 0.001$). Interestingly, at 2-week age, cartilage from *Col3a1*$^{+/-}$ mice also had reduced modulus (0.7 ± 0.5 MPa versus 1.3 ± 0.2 MPa in WT, $n = 5$, $p = 0.016$), albeit to a lesser extent (45 ± 6 %). Comparing the two ages, we found an age-associated modulus increase in WT cartilage (1.7 ± 0.1 fold from 2-week to 2-month age, $p < 0.01$), illustrating the expected matrix stiffening during skeletal maturation [20]. However, such trend was absent in *Col3a1*$^{+/-}$ cartilage ($p = 0.876$), suggesting that collagen III may be critical for the post-natal maturation of cartilage. For the meniscus, *Col3a1*$^{+/-}$ tissues also had lower modulus than that of WT at 2-month age (2.1 ± 0.8 MPa versus 3.7 ± 1.2 MPa, $n = 7$, $p = 0.028$), but not at 2-week age (0.9 ± 0.5 MPa versus 1.1 ± 0.2 MPa in WT, $n = 5$, $p = 0.548$, Fig. 2b).

Given that collagen III is more concentrated in cartilage PCM (Fig. 1b), we further tested if collagen III deficiency impaired the local micromechanical properties of the PCM in 2-month-old cartilage, using our recently established, immunofluorescence (IF)-guided AFM nanomechanical mapping in combination with Kawamoto's film-assisted cryo-sectioning [44, 45]. Here, reduction of collagen III did not significantly change the thickness of the PCM (Fig. 3a, b, ≥ 120 cells from $n = 6$ animals, $p = 0.448$), as measured from the IF images of collagen VI, one biomarker of cartilage PCM [46, 47]. Guided by the IF-labelling of collagen VI, we separated the micromodulus of the PCM and the T/IT-ECM (Fig. 3c). In both genotypes, as expected [48], the PCM had lower modulus than the T/IT-ECM. Also, consistent with the contrast observed at the tissue-level,

cartilage of *Col3a1*$^{+/-}$ mice showed significantly lower micromodulus than that of WT mice in both the PCM and T/IT-ECM (≥ 12 regions of interest (ROIs) from $n = 6$ animals, > 600 locations for PCM, $p = 0.004$; > 2,800 locations for T/IT-ECM, $p = 0.015$, Fig. 3d).

2.3 Reduction of collagen III leads to thickened collagen fibrils with increased heterogeneity.

We also detected significant changes in collagen fibril nanostructure on the surface (Fig. 4) and in the matrix interior of both articular cartilage (Fig. 5) and meniscus (Fig. 6) in *Col3a1*$^{+/-}$ mice. Consistent with the literature, the cartilage surface in both genotypes was characterized by transversely random fibrils [49], while the meniscus surface was dominated by circumferentially aligned fibrils [36] (Fig. 4a). On the surface of *Col3a1*$^{+/-}$ cartilage, there was a significant increase in fibril diameter at 2-month age ($p < 0.001$, ≥ 200 fibrils by SEM from $n = 5$ animals), but not at 2-week age ($p = 0.257$), as measured by SEM (Fig. 4; Table 1). On the other hand, we did not detect significant changes in fibril heterogeneity on the surface (F-test, $p = 0.539$ for 2-week age, $p = 0.060$ for 2-month age, data not shown). This thickening effect was also observed in the middle/deep zone interior, and present in both the PCM and the T/IT-ECM, as measured by TEM ($p < 0.001$, ≥ 130 fibrils from $n = 4$ animals for each domain, Fig. 5a, b; Table 2). Meanwhile, reduction of collagen III also significantly increased fibril heterogeneity in both the PCM and T/IT-ECM (F-test, $p < 0.001$, Fig. 5c). In 2-month-old WT cartilage, the T/IT-ECM had significantly thicker collagen fibrils compared to the PCM, as expected ($p < 0.001$), while such contrast was absent in *Col3a1*$^{+/-}$ cartilage ($p = 0.170$), illustrating the impaired fibril growth from the PCM to the T/IT-ECM in the deficiency of collagen III (Table 2).

Similar to the case of cartilage, *Col3a1*$^{+/-}$ meniscus at 2-month age also exhibited fibril thickening both on the surface ($p < 0.001$, ≥ 200 fibrils, $n = 5$, Fig. 4) and in the interior ($p < 0.001$, ≥ 600 fibrils, $n = 4$, Fig. 6a, b). On the surface, there was no significant change in the fibril heterogeneity (F-test, $p = 0.133$, data not shown). However, in the interior, there was a substantial increase in fibril diameter heterogeneity ($p < 0.001$, Fig. 6c) and decrease in fibril number ($p < 0.001$, Fig. 6d). Moreover, the distribution of *Col3a1*$^{+/-}$ meniscus collagen fibrils showed a distinctive bimodal distribution (bimodality coefficient $b = 0.57 > 0.55$, the threshold

for bimodality [50]), whereas the second frequency peak signified substantially thickened fibrils (μ_2 = 158.3 nm, Fig. 6b). This was different from the collagen fibril diameter distributions of in the meniscus of WT mice (b = 0.44) and in the cartilage of both genotypes, all of which could be described by the unimodal normal distribution.

2.4 Reduction of collagen III leads to increased amount of collagen cross-links.

According to the amino acid analysis, WT and *Col3a1*$^{+/-}$ tissues had similar total collagen content (Fig. 7a) and the extent of lysine hydroxylation of collagen (data not shown). From the collagen cross-link analyses, three major cross-link types were identified in articular cartilage, one immature, reducible type, dihydroxylysinonorleucine (DHLNL), and two mature, non-reducible types, pyridinoline (Pyr, or hydroxylysyl pyridinoline) and deoxypyridinoline (d-Pyr, or lysyl pyrodinoline). In the meniscus, DHLNL and Pyr were also detected, while d-Pyr was absent. For articular cartilage, *Col3a1*$^{+/-}$ tissue had significantly higher amount of both reducible (DHLNL) and non-reducible (d-Pyr) cross-links than WT (n = 4 biological repeats, $p < 0.05$, Fig. 7b), but similar amount of Pyr cross-links (p = 0.250). For the meniscus, *Col3a1*$^{+/-}$ tissue had significantly higher amount of both DHLNL and Pyr cross-links ($p < 0.01$, n = 3, Fig. 7b). Collectively, *Col3a1*$^{+/-}$ tissues had higher amount of total aldehydes, which are required for the formation of collagen intermolecular cross-links, and are generated by the action of lysyl oxidase (LOX) [51]. Interestingly, despite this increase in total aldehydes and collagen cross-links, we did not detect significant changes in the overall LOX content in both articular cartilage (p = 0.112) and the meniscus (p = 0.779) in comparison to the WT control, as measured by western blot (Fig. 7c).

2.5 Reduction of collagen III does not markedly alter subchondral bone structure.

Given the importance of the subchondral bone in maintaining joint health [52], we assessed the structure of subchondral bone plate (SBP) and subchondral trabecular bone (STB) using micro-computed tomography (μCT, n = 5) (Fig. 8). We did not find significant differences in their structural parameters, including SBP thickness, STB bone volume fraction (BV/TV), trabecular number (Tb.N), thickness (Tb.Th) and separation

(Tb.Sp). The absence of structural phenotype in the regions of SBP and STB suggests that reduction of collagen III does not directly affect the formation of bony tissues in these specific regions of young male mice examined in this study. Therefore, the observed phenotype in articular cartilage and meniscus is less likely to be a secondary effect arising from subchondral bone abnormalities.

3. Discussion

3.1 Role of collagen III in cartilage matrix structure and mechanical properties

This study shows that type III collagen is a crucial matrix constituent for the establishment of normal cartilage ECM. According to the outcomes from sGAG-removed cartilage, which represents mechanical properties associated with the collagen fibrillar network, the lower modulus of *Col3a1*$^{+/-}$ tissue (Fig. 2a) signifies the impairment of collagen fibril structural integrity with the deficiency of collagen III. The biomechanical outcomes (Fig. 2a) thus provide direct evidence supporting the hypothesis proposed by Eyre and co-workers, that is, collagen III functions as a covalent fibril network modifier that strengthens the collagen II fibrillar network [19]. In cartilage, most collagen III molecules retain the cysteine-rich N-propeptides during post-translational modification [19] (Fig. 9a). The pN-collagen III molecules primarily co-assemble on the surfaces of collagen II fibrils, and form covalent cross-links with both collagen II and other collagen III molecules at the N- and C-telopeptides as well as the triple helix domain (Lys^{87} and Lys^{930}) [19]. It is suggested that in cartilage, collagen III also exists in the form of thin filamentous polymers of pN-collagen III molecules cross-linked head-to-tail at 4D-staggered sites, which are cross-linked laterally with collagen II fibril surfaces to act as a "molecular glue", thereby enhancing inter-fibrillar cohesion [19]. Moreover, our observation on the nanostructural phenotype of *Col3a1*$^{+/-}$ cartilage (Figs. 4, 5) suggests that collagen III not only acts to strengthen the collagen fibrillar network, but also maintains the fibril homogeneity and limits aberrant fibril thickening. It is possible that by covalently cross-linking with collagen II on fibril surfaces, collagen III effectively inhibits further lateral growth of fibrils. In addition, the non-helical N-propeptides could accumulate on fibril surfaces to provide steric hindrance, further limiting fibril lateral growth [53] (Fig. 9a). Collectively, collagen III mediates

the assembly of collagen II fibrils in a manner similar to its canonical function in limiting the formation of thickened collagen I fibrils in other fibrous tissues [4, 16, 17], and its contribution is crucial to establishing the structural integrity and biomechanical functions of normal cartilage ECM during post-natal growth (Fig. 9b).

In addition to its influence on the collagen fibrillar network, collagen III also impacts the contribution of aggrecan and its sGAGs to cartilage biomechanics. While collagen III does not directly influence the sGAG content (Fig. 1c, d), the magnitude of modulus contributed by sGAGs to cartilage ($E_{\text{ind, sGAGs}} \approx E_{\text{ind, untreated}} - E_{\text{ind, C'ABC}}$) is decreased with the reduction of collagen III (≈ 0.63 MPa for *Col3a1*$^{+/-}$ versus ≈ 1.60 MPa for WT, Fig. 2). This effect can also be attributed to the impairment of collagen fibril structure. In cartilage, the GAG-GAG spacing of aggrecan (≈ 2-5 nm) is comparable to the Debye length (≈ 1 nm), which renders the molecular mechanics of aggrecan to be highly sensitive to its nanoscale conformation [54, 55]. In the ECM, the porous collagen fibrillar network entraps the aggrecan-HA aggregates to establish the highly compressed aggrecan conformation, i.e., a ≈ 50% compressive molecular strain even in unloaded cartilage [20]. The weakened collagen fibrillar network due to collagen III deficiency could have decreased capability of confining the highly compressed aggrecan molecules (Fig. 9b). Here, our results show that the altered conformation of aggrecan, as a result of collagen III deficiency, leads to largely reduced $E_{\text{ind, sGAGs}}$ (Fig. 2a), supporting the hypothesis that aggrecan possibly experiences lower molecular compressive strain in *Col3a1*$^{+/-}$ cartilage.

3.2 Contribution of collagen III to the micromechanics of cartilage pericellular matrix

In cartilage matrix, the PCM is the structurally distinctive, ~ 2-5 μm-thick microdomain that is in immediate contact with chondrocytes [40]. Being the ECM-cell interface, the PCM plays pivotal roles in sequestering growth factors [56], transducing mechanoelectrochemical signals [57, 58] and protecting cells from overloading [59, 60], which together regulate the homeostasis of healthy cartilage. In healthy cartilage, collagen III is more concentrated in the PCM [30, 42] (Fig. 1b). Since the PCM is also where the initial matrix molecular assembly occurs [61], collagen III is poised to play a role in mediating the initial stage of collagen II/IX/XI fibril formation. Here, reduction of collagen III significantly decreases the micromodulus of the PCM

(Fig. 3), and has a more pronounced impact on the fibril nanostructure in the PCM (48 ± 9 % increase in d_{col}) than in the T/IT-ECM (16 ± 7 % increase) (Fig. 5). On the other hand, since the formation of the T/IT-ECM depends on the initial fibril assembly in the PCM, the disrupted fibril structure of the PCM in *Col3a1*$^{+/-}$ mice thus also alters the fibril structure in the T/IT-ECM (Figs. 3, 5). Moreover, the PCM has higher concentrations of proteoglycans such as aggrecan, decorin, biglycan and perlecan [62], indicating that the PCM has higher local molecular compression and osmotic swelling pressure than the T/IT-ECM. The higher concentration of collagen III in the PCM could thus strengthen the collagen II fibril network's capability of confining and retaining the highly compressed proteoglycans, overcoming the challenge that collagen II fibrils are thinner and weaker in the PCM. Given the fast turnover of collagen III in vivo [31], its possible involvement in OA pathology [30, 32] and its preferential distribution in the PCM (Fig. 1b), collagen III could potentially function as a transient repair collagen, which temporarily stiffens the PCM in OA or regeneration. This role can protect chondrocytes from overloading and influence the homeostatic balance of chondrocyte metabolic activities in response to their micromechanical niche, i.e., the PCM. We thus hypothesize that a more comprehensive description of the collagen fibrillar network in cartilage ECM is a collagen II/III/IX/XI heterotypic network (Fig. 9), in which, the content and participation of collagen III could vary markedly with development and disease. We further hypothesize that the role of collagen III is to regulate collagen II fibril structural integrity, aggrecan molecular conformation, and thus, normal cartilage biomechanical functions and chondrocyte mechanotransduction.

3.3 Comparison of collagen III contributions to the matrices of articular cartilage and meniscus

For the meniscus, the increase in fibril diameter and heterogeneity, and decrease in fibril density and tissue modulus with collagen III reduction (Figs. 2, 4, 6), are in alignment with the known activities of collagen III in mediating collagen I fibrillogenesis [4, 16, 17]. Notably, the appearance of much thickened fibrils (μ_2 = 158.3 nm in the bimodal distribution) and the substantial reduced amount of thinner fibrils (< 30 nm) in *Col3a1*$^{+/-}$ meniscus (Fig. 6b) highlight the role of collagen III in limiting aberrant fibril thickening. In

comparison, while cartilage also shows reduced amount of thin fibrils, the much thickened fibrils are absent in cartilage matrix (Fig. 5b). This could be attributed to the lower inherent capability of collagen II in forming dramatically thickened fibrils [63], as well as the presence of highly concentrated proteoglycans that provide interfibrillar spacing and limit fibril overgrowth [62]. In addition, while the hypothesized collagen III thin filamentous network is originally proposed in cartilage [19], it is possible that collagen III also plays a similar role in strengthening the collagen I fibers, given its ability of retaining the N-propeptides and forming covalent cross-links on collagen I fibril surfaces [16]. Therefore, in both articular cartilage and meniscus, collagen III limits fibril thickening during development in both cartilage and meniscus, and has a more pronounced impact on the biomechanics of articular cartilage (Fig. 2). One possible explanation is that in cartilage, collagen III could impact not only the collagen fibril nanostructure, but also the molecular conformation of aggrecan integrated within the collagen fibrillar network.

3.4 Correlation between collagen cross-linking and tissue modulus

In both articular cartilage and meniscus, we show that reduction of collagen III leads to decreased tissue modulus (Fig. 2), despite the increase in collagen cross-link density (Fig. 7b). Here, the increased cross-linking in collagen III-deficient tissues potentially relates to its effect on fibril thickening. Cross-linking of collagen is initiated by the conversion of lysine or hydroxylysine residues in telopeptides to aldehydes catalyzed by the action of LOX and its isoforms [51]. A previous study showed that LOX is active on the aggregate of collagen molecules on fibrillar surfaces, but not on collagen monomers [64]. The thickening of fibrils, as a result of collagen III deficiency, could increase the binding of LOX, and thus, LOX-mediated conversion of aldehydes and subsequent formation of cross-links. It is also possible for collagen III to undergo different paths of post-translational modifications from collagen II, thereby leading to a change in the cross-link pattern within the fibril network. Meanwhile, the absence of changes in LOX protein level under collagen III deficiency (Fig. 7c) supports that collagen III regulates the activities of LOX by mediating fibril structure, organization and possibly cross-linking pattern, rather than by increasing the level of LOX proteins.

The finding that tissue modulus does not positively correlate with cross-link density may seem counter intuitive. However, it emphasizes that tissue mechanical properties are an integrated manifestation of both the composition and hierarchical structure of the matrix [65]. The moduli of both cartilage and meniscus are governed by not only the amount of collagen cross-links, but many other factors, such as cross-linking pattern (e.g. molecular distribution, intra- versus inter-fibrillar cross-links), fibril organization, packing and collagen-proteoglycan integration. Under the deficiency of collagen III, although increased cross-link density may stiffen individual collagen fibrils, many other phenotypic changes could contribute to the reduced tissue modulus. These include the disruption of collagen fibril nanostructure, impairment of cross-linking patterns, possible reduction of the strengthening effect from the collagen III filamentous network, and in cartilage, possible decrease of aggrecan molecular strain. All these changes can alter matrix deformation modes at the nanoscale, such as fibril bending, uncrimping, sliding, and in cartilage, electrical double layer repulsion associated with aggrecan compression. Thus, with regards to the net impact of collagen III deficiency on tissue biomechanics, our results show that these structural defects outweigh the effect of increase in cross-linking.

Our results corroborate with the literature suggesting that while collagen cross-linking is an important determinant of tissue integrity, the cross-link density alone is not a direct indicator of tissue modulus. Amongst different connective tissues, the ones with highest collagen cross-link densities do not have the highest modulus, i.e., the nucleus pulposus [66]. Here, we also show that articular cartilage has lower modulus than the meniscus, despite having higher cross-link density (Figs. 2, 7). Within the same tissue type, cross-link density alone also does not positively correlate with tissue modulus. For example, fibromodulin-null tendon develops weakened tensile modulus despite having increased collagen cross-linking than the WT control. This is attributed to the altered cross-linking pattern, where under the loss of fibromodulin-modulated site-specific collagen cross-linking, a higher portion of cross-links are formed at the C-telopeptide, resulting in impaired integrity of cross-links [67]. To this end, although a clear, positive correlation between modulus and cross-linking is reported in developing embryonic tendon [68], this stiffening effect is also accompanied with other structural changes during development, such as increased collagen deposition and organization. In adult tendons, even without

genetic perturbation of matrix structure, correlation between modulus and cross-linking is weak and inconclusive [69, 70].

3.5 Limitations and outlook

It is worth noting that we did not detect marked gross-level phenotype in *Col3a1*$^{+/-}$ cartilage via histology (Fig. 1d), despite the significant changes in matrix nanostructure and biomechanical properties. This could be attributed to the fact that this study mainly focuses on young mice (up to 2-month age). It is possible that longer term studies in aged mice will reveal the development of gross pathology associated with the disturbances in tissue structure and biomechanics. In fact, vEDS patients without a familial history are typically not diagnosed until the fourth decade of life [71]. Furthermore, while this study did not detect significant phenotype in the subchondral bone of young male mice (Fig. 8), given that subchondral bone development is sex-dependent [52], we cannot rule out the possibility that loss of collagen III could affect the subchondral bone in female mice or at older ages. In fact, female *Col3a1*$^{+/-}$ mice are known to develop significant structural defects in the distal femur trabecular bone at both young adult and old ages [12]. Moreover, while this study focuses on normal joint maturation, collagen III could play an even more substantial role in tissue remodeling and degeneration during aging and post-traumatic disease progression [32, 42, 72]. Our ongoing studies thus aim to establish tissue-specific *Col3a1* knockout mice, which will enable us to delineate collagen III activities at different ages, and to separate its roles in normal homeostasis, disease and associated repair processes.

4. Conclusions

This study highlights that type III collagen is a crucial structural constituent of both collagen I-dominated meniscus and collagen II-rich articular cartilage. In both tissues, collagen III maintains fibril homogeneity and limits aberrant fibril thickening, and in cartilage, such effect could also influence the integration of aggrecan network (Fig. 9). In cartilage, the influence of collagen III is more pronounced in the PCM, which indicates potential roles of collagen III in early fibrillogenesis, as well as in chondrocyte mechanotransduction. Notably, while reducing collagen III increases collagen cross-link density, it decreases

tissue modulus resulting from the pronounced structural defects. In summary, our results extend current understanding of collagen III structural roles in matrix assembly, as well as the composition-structure-function relationships of articular cartilage and meniscus. Building on this study, we expect that an in-depth understanding of collagen III will provide a new basis for improving cartilage and meniscus regeneration by modulating collagen III-directed molecular and cellular responses.

5. Methods

5.1 Animal model

Animal use and care were approved by the Institutional Animal Care and Use Committee (IACUC) at the University of Pennsylvania, following the NIH Guide for the Care and Use of Laboratory Animals. All mice used in this study were generated from the breeding pairs of *Col3a1* heterozygous (*Col3a1*$^{+/-}$) mice in the BALB/c strain (Jackson Laboratories, Bar Harbor, ME). These mice were generated by homologous recombination via replacing the promoter region and first exon of the *Col3a1* gene with a 1.8-kb PGK neo-cassette [4], generating a global knockout of *Col3a1*. All the animals used here were genotyped for *Col3a1* by PCR of DNA extracted from tail biopsy specimens and were microchipped for identification (AllflexFDX-B transponders, Allflex, Dallas, TX).

Two-week and two-month old wild-type (WT) and *Col3a1*$^{+/-}$ male mice were chosen for this study. The null mice (*Col3a1*$^{-/-}$) were not included due to their high perinatal lethality [4, 14]. For morphological analyses, for each mouse, either the left or the right side of the hind knee joint was chosen for μCT scanning after fixation, then processed for histology. Articular cartilage and meniscus were harvested from the other side of the knee joint. They were first used for AFM-nanomechanical tests, and then, processed for surface collagen fibril structure analysis via scanning electron microscopy (SEM). Femoral head cartilage from the same mice was used for sGAG content quantification. Additional mice were used for transmission electron microscopy (TEM), quantitative RT-PCR (qPCR) analysis, western blot and collagen cross-linking analyses. For qPCR, sGAG, western blot and cross-linking analyses, each biological repeat consists of 6 femoral head cartilage tissues or the non-ossified central region of 12 menisci pooled from 3 mice of the same age and genotype.

5.2 Histology, immunohistochemistry and sGAG analysis

Knee joints were fixed in 4% paraformaldehyde (PFA) for 24 hrs, decalcified in 10% EDTA for 7 days for 2-week-old joints and 21 days for 2-month-old joints. Paraffin-embedded samples were sectioned into 6-μm-thick slices at the sagittal plane, then stained by Safranin-O/Fast Green to assess the joint and cell morphology as well as gross-level staining of sGAGs ($n \geq 6$). The thicknesses of uncalcified and total cartilage were quantified from Safranin-O/Fast Green images with a distinctive tidemark. In brief, for each section, a region of interest (ROI) was defined in the each of the anterior, middle and posterior regions of both femur and tibia joints. For each ROI, the uncalcified and total cartilage thicknesses were measured within an ~ 100 μm-long cartilage surface using ImageJ. The mean cartilage thickness of each animal was calculated by averaging measurements from three sections spaced ~ 50 μm apart [73]. For immunohistochemistry (IHC) ($n = 5$), paraffin-embedded sections were incubated in 60°C for 1 hr, deparaffinized and rehydrated with xylene and series-diluted ethanol-water solutions, treated with 0.1% pepsin (P7000, Sigma, Milwaukee, WI) at 37°C for 10 min to retrieve antigen, quenched endogenous peroxidase activity with 3% H_2O_2 in methanol, blocked with 5% BSA, 1% Goat Serum in PBS, followed by avidin-biotin blocking (SP-2001, Vector Laboratories, Burlingame, CA), then incubated with primary antibody (collagen III: AB7778, Lot #GR191100-2, 1:1000 dilution, Abcam, Cambridge, MA) at 4°C overnight. Next day, sections were washed with PBS, then incubated with secondary antibody (65-6120, 1:1000 dilution, ThermoFisher, Foster City, CA) at room temperature for 1 hr and vectastain ABC (PK-7200, Vector Laboratories) at room temperature for 30 min, respectively. Sections were then incubated with DAB (ImmPACT SK-4105, Vector Laboratories) for 5-10 min, counter-stained with hematoxylin, and dehydrated with series-diluted ethanol-water solutions and xylene, prior to mounting and imaging. Internal negative control was prepared following the same procedures except without the primary antibody incubation. For sGAG quantification, femoral head cartilage was digested overnight at 60°C in papain mixture (2% papain, 10 mM Cysteine HCl, 63.6 mM EDTA, 0.1M sodium acetate trihydrate), and analyzed via the standard dimethylmethylene blue dye assay (DMMB) [74].

5.3 Quantitative RT-PCR

Quantitative reverse transcriptase polymerase chain reaction (qRT-PCR, or qPCR) was performed on both femoral head cartilage and meniscus from 2-month old mice. RNA extraction was performed by homogenizing tissue in TRI-reagent and phase-separated in 1-bromo-3-chloropropane. RNA quality was assessed using the NanoQuant Plate (Tecan, Switzerland) with the Infinite 200 plate reader. Total RNA (3 ng per well) was subjected to reverse transcription using the TaqMan reverse transcription kit (N8080234, ThermoFisher), with amplification carried out via the PowerUp SYBR Green Master Mix (A25742, ThermoFisher) on a RealPlex 4S master cycler (Eppendorf AG, Hamburg, Germany). The primer sequences used in this study were listed in Table 3.

5.4 Biomechanical analyses via AFM-nanoindentation

To quantify the tissue-level modulus of articular cartilage and meniscus, AFM-nanoindentation was performed on the surfaces of freshly dissected medial condyle cartilage, and the non-ossified, central region of medial meniscus. All the tests were performed via colloidal microspherical tips ($R \approx 5$ μm, nominal $k \approx 5.4$ N/m, HQ: NSC35/tipless/Cr-Au, cantilever B, NanoAndMore, Lady's Island, SC) and a Dimension Icon AFM (Bruker Nano, Santa Barbara, CA). For each sample, at least 10 different locations on the load bearing regions were randomly tested to account for spatial heterogeneity. At each location, an indentation force versus depth (*F-D*) curve was obtained at the indentation rate ≈ 10 μm/s. The effective indentation modulus, E_{ind}, was calculated by fitting the entire loading portion of each *F-D* curve to the Hertz model [49] with the Poisson's ratio assumed to be 0.1 for cartilage [75] and 0 for meniscus [76]. To assess the direct contribution of sGAGs on aggrecan to cartilage modulus, additional freshly dissected joints were treated with 0.1 U/mL chondroitinase-ABC (C962T85, Sigma) for 48 hrs [77] at 37°C to remove GAGs and non-fibrillar proteins and tested under AFM. Throughout the AFM experiments, samples were immersed in phosphate buffered saline (PBS) with protease inhibitors (Pierce 88266, Fisher Scientific, Rockford, IL) at room temperature to minimize post-mortem degradation.

To quantify the micromechanical properties of cartilage PCM and T/IT-ECM, freshly dissected tibia joints were embedded in optimal cutting temperature medium, and cryotomed to produce ≈ 6-μm-thick, unfixed sagittal cryo-sections via Kawamoto's film method [44]. Each cryo-section was immuno-labelled with collagen VI, the biomarker of cartilage PCM [46]. Briefly, cryo-sections were washed by PBS to remove surrounding OCT, blocked with 5% BSA and 1% Goat Serum for 30 min, incubated with collagen VI primary antibody (1:50, 70R-CR009X, Fitzgerald, Acton, MA) for 20 min at room temperature, followed by incubation of secondary antibody (1:200, A-11037, ThermoFisher) for 20 min at room temperature, and then, immediately used for AFM tests. Guided by the collagen VI IF-imaging, AFM-nanomechanical mapping was performed using microspherical tips ($R \approx 2.25\mu m$, $k \approx 1$ N/m, HQ:NSC36/tipless/Cr-Au, NanoAndMore) and an MFP-3D AFM (Asylum Research, Santa Barbara, CA) in PBS with protease inhibitors. For each map, a 40 × 40 indentation grid was acquired over a 20 × 20 μm^2 ROI containing well-defined, circular PCM terrains [45]. The effective indentation modulus, E_{ind}, was calculated via the finite thickness-corrected Hertz model [78]. In addition, the thickness of PCM was measured on the collagen VI IF images using ImageJ (n = 6 mice per genotype, ≥ 20 cells per animal).

5.5 Collagen nanostructural analysis

To assess the collagen fibril nanostructure on tissue surfaces, immediately after AFM test, femoral condyle and meniscus were treated with 0.1% trypsin (T7409, Sigma) and 0.1% hyaluronidase (H3506, Sigma) at 37°C for 24 hrs, respectively. Samples were then fixed with fresh Karnorsky's fixative (Electron Microscopy Sciences, Hatfield, PA) at room temperature for 3 hrs, dehydrated in a series of graded water-ethanol (water/ethanol ratio: 3/1 to 1/1 to 1/3 to 0/1) and ethanol-hexamethyldisilazane (HMDS, A15139, Alfa Aesar, Tewksbury, MA) (ethanol/HMDS ratio: 3/1 to 1/1 to 1/3 to 0/1) mixtures, and air dried overnight [79]. SEM (Zeiss Supra 50VP, Germany) images were acquired on samples coated with ≈ 6 nm thick platinum.

To quantify the collagen fibril nanostructure in matrix interior, freshly dissected tibia and meniscus were fixed in fresh Karnovsky's fixative for 15 min in room temperature, then placed on orbital shaker with gentle

movement for 2 hrs at 4°C. Samples were sent to the University of South Florida (USF) for TEM imaging via overnight shipping. During shipment, menisci were kept in fixation solution on ice, while tibias were transferred during the decalcification process, which started 10 days before the shipping. Upon arrival, samples were rinsed with sodium cacodylate buffer and post-fixed for 1 h with 1% osmium tetroxide, dehydrated in an ethanol series followed by 100% propylene oxide, infiltrated and embedded over a 3 day period in a mixture of Embed 812, nadic methyl anhydride, dodecenylsuccinic anhydride and DMP-30 (EM Sciences, Fort Washington, PA) and polymerized overnight at 60 °C. Ultra-thin, approximately 90 nm, cross-sections were prepared using a Leica ultramicrotome and post-stained with 2% aqueous uranyl acetate and 1% phosphotungstic acid, pH 3.2. The sections were examined and imaged at 80 kV using a JEOL 1400 TEM (JEOL, Tokyo, Japan) equipped with a Gatan Orius widefield side mount CCD camera (Gatan Inc., Pleasanton, CA) [80]. Based on the SEM and TEM images, collagen fibril diameter, heterogeneity and density were quantified via ImageJ by two independent researchers.

5.6 Amino acid and collagen cross-linking analysis

Femoral head cartilage and the central, non-mineralized region of meniscus (with the two mineralized horns removed) of mice were stored in dry ice and used for amino acid analysis and cross-linking analysis, following established procedures [81]. In brief, samples were pulverized, reduced with standardized NaB^3H_4, hydrolyzed with 6N HCl and subjected to amino acid and cross-link analyses. Collagen content was calculated as a percentage of total proteins based on the value of 100 residues of hydroxyproline per 1,000 total amino acids in collagen. The extent of lysine hydroxylation of collagen was calculated on the basis of 300 hydroxyproline residues per collagen. For cross-link analysis, the reducible cross-links/aldehydes were measured as their reduced forms, e.g. dehydrodihydroxylysinonorleucine (deH-DHLNL)/its ketoamine as DHLNL by radioactivity, and non-reducible cross-links pyridinoline (Pyr) and deoxypyridinoline (d-Pyr), by fluorescence. The amount of cross-links was quantified and expressed as mol per mol of collagen via

normalization to hydroxylproline content. The total number of aldehydes involved in the detected cross-links was calculated as the sum of (DHLNL + 2 × Pyr + 2 × d-Pyr) [82].

5.7 Western blot analyses

Femoral head cartilage and meniscus from 2-month old mice were used to assess the level of LOX in both genotypes. Protein extraction was performed by homogenizing tissue in TRI-reagent and phase-separated in 1-bromo-3-chloropropane. BCA Assay Kit was used to quantify the protein concentration. Tissue lysates with 10 µg protein mixed with reducing agent and LDS sample buffer were loaded on a 4-12% Bis-Tris gel. Separated protein was transferred onto a polyvinylidene fluoride (PVDF) membrane (IB401002, ThermoFisher) with an iBlot mini transfer stack (IB401002, ThermoFisher). The PVDF membrane was blocked for 1 hr in TBST with 5% non-fat milk and 1% BSA. The membrane was then incubated with primary antibodies (LOX: NBP2-24877, 1:100 dilution, Novus Biologicals, Centennial, CO; GAPDH: 14C10, 1:500, Cell Signaling Technology, Danvers, MA) in the same blocking buffer at 4ºC overnight, followed by the incubation of secondary antibody (65-6120, 1:1,000 dilution, ThermoFisher) for 1 hr at room temperature. The development was performed with the Pierce ECL Plus Western Blotting Substrate (32132, ThermoFisher) and imaged with a FluorChem M system (ProteinSimple, San Jose, CA). Densitometry was quantified using Image Studio Lite, and the level of each LOX content was normalized to its internal control, GAPDH. In addition, to validate the specificity of the collagen III antibody, recombinant human collagen I (C7624, Sigma) and collagen III (ab73160, Abcam), extracted human collagen II from articular cartilage (009-001-104, Rockland, Limerick, PA) were subjected to western blot analysis. In brief, after BCA assay, 1, 2, and 5 µg of each collagen type respectively mixed with reducing agent and LDS sample buffer were loaded on a 4-12% Bis-Tris gel, transferred to PVDF membrane, blocked by non-fat milk, and incubated with primary antibody (Abcam 7778, 1:500, Lot #GR3261539-1), following the same procedure.

5.8 Micro-computed tomography (µCT)

The same knee joints purposed for histology were scanned by ex vivo μCT (microCT 35, Scanco Medical AG, Brüttisellen, Switzerland) in 4% PFA solution before decalcification. A ~ 3 mm region from the distal femur and the proximal tibia were scanned at a 6-μm isotropic voxel size. All images were smoothed by a Gaussian filter (sigma = 1.2, support = 2.0) and the threshold corresponding to 30% of the maximum available range of image gray scale values. For subchondral bone plate (SBP) analysis [83], SBP at the load bearing region in sagittal images were contoured to calculate the SBP thickness (SBP.Th). For subchondral trabecular bone (STB) analysis on the medial side of tibia, bone volume fraction (BV/TV), trabecular number (Tb.N), trabecular bone thickness (Tb.Th) and separation (Tb.Sp) were calculated by the standard 3D microstructural analysis [84].

5.9 Statistical analysis

To compare the tissue biomechanical properties between the two genotypes, Mann-Whitney U test was applied to the average E_{ind} values of each animal, for both whole-tissue tests and IF-guided micromechanical tests. In addition, unpaired two sample student's *t*-test was applied to examine the differences in cartilage thicknesses, sGAG amount, collagen and collagen cross-linking contents, LOX content, PCM thickness, as well as μCT outcomes. For collagen structural data, since ≥ 200 fibrils were measured for each region and each genotype, based on the central limit theorem, two-sample *z*-test was applied to compare the mean fibril diameters, and *F*-test was applied to compare the fibril diameter variances. In addition, bimodality coefficient was estimated to determine if each fibril sample conformed to a unimodal or bimodal distribution at the threshold of 5/9 [50]. In all the tests, the significance level was set at $\alpha = 0.05$.

Author Contributions

Conceptualization, L.H., S.V.W. and C.W.; Supervision, L.H., S.V.W. and M.Y.; Data Collection and Analysis, C.W., B.K.B., M.T., Q.L., K.H., B.H., A.M.G. and M.E.-I.; Data Interpretation: C.W., B.K.B., M.T., X.S.L., M.S.M., M.E.-I., M.Y., S.V.W. and L.H.; Writing, C.W., B.K.B., M.Y., S.V.W. and L.H.; Funding Acquisition: L.H. and S.V.W. All authors intellectually contributed and provided approval for publication.

Acknowledgments

This work was financially supported by the National Science Foundation (NSF) Grant CMMI-1751898 (to LH), Drexel Area of Research Excellence (DARE) Award (to MSM and LH), National Institutes of Health (NIH) Grant R01GM124091 (to SWV), the Penn Center for Musculoskeletal Disorders (PCMD) Pilot Grant (to SWV and LH), as well as NIH Grant P30AR069619 to the PCMD. We thank Dr. David E. Birk and Sheila M. Adams (University of South Florida) for the kind help with the TEM imaging, Dr. David R. Eyre (University of Washington) for insightful discussions, as well as the Singh Center for Nanotechnology at the University of Pennsylvania for the use of TIRF MFP-3D.

Abbreviations Used

3D, Three dimensional; AFM, atomic force microscopy; C'ABC, chondroitinase ABC; deH-DHLNL, dehydrodihydroxylysinonorleucine; de-Pyd, deoxy-pyrodinoline; DHLNL, dihydroxylysinonorleucine; DMMB, dimethylmethylene blue; ECM, extracellular matrix; HMDS, hexamethyldisilazane; IF, immunofluorescence; IHC, immunohistochemistry; OA, osteoarthritis; LOX, lysyl oxidase; MFP, molecular force probe; PBS, phosphate buffered saline; PCM, pericellular matrix; PFA, paraformaldehyde; PVDF, polyvinylidene fluoride; Pyd, pyrodinoline; qRT-PCR, quantitative reverse transcriptase polymerase chain reaction; SBP, subchondral bone plate; SEM, scanning electron microscopy; sGAG, sulfated glycoaminoglycan; STB, subchondral trabecular bone; T/IT-ECM, territorial/interterritorial extracellular matrix; TEM, transmission electron microscopy; TIRF, total internal reflection fluorescence; vEDS, vascular Ehlers-Danlos syndrome; WT, wild-type; μCT, micro-computed tomography.

References

[1] S.P. Boudko, J. Engel, K. Okuyama, K. Mizuno, H.P. Bachinger, M.A. Schumacher, Crystal structure of human type III collagen Gly^{991}-Gly^{1032} cystine knot-containing peptide shows both 7/2 and 10/3 triple helical symmetries, J. Biol. Chem. 283 (47) (2008) 32580-32589.

[2] K. Niederreither, R. D'Souza, M. Metsaranta, H. Eberspaecher, P.D. Toman, E. Vuorio, B. De Crombrugghe, Coordinate patterns of expression of type I and III collagens during mouse development, Matrix Biol. 14 (9) (1995) 705-713.

[3] W. Henkel, R.W. Glanville, Covalent crosslinking between molecules of type I and type III collagen. The involvement of the N-terminal, nonhelical regions of the alpha 1 (I) and alpha 1 (III) chains in the formation of intermolecular crosslinks, Eur. J. Biochem. 122 (1) (1982) 205-213.

[4] X. Liu, H. Wu, M. Byrne, S. Krane, R. Jaenisch, Type III collagen is crucial for collagen I fibrillogenesis and for normal cardiovascular development, Proc. Natl. Acad. Sci. U. S. A. 94 (5) (1997) 1852-1856.

[5] P.H. Byers, J. Belmont, J. Black, J. De Backer, M. Frank, X. Jeunemaitre, D. Johnson, M. Pepin, L. Robert, L. Sanders, N. Wheeldon, Diagnosis, natural history, and management in vascular Ehlers-Danlos syndrome, Am. J. Med. Genet. C Semin. Med. Genet. 175 (1) (2017) 40-47.

[6] P.H. Byers, Vascular Ehlers-Danlos Syndrome. 1999 Sep 2 [Updated 2019 Feb 21], in: M.P. Adam, H.H. Ardinger, R.A. Pagon, S.E. Wallace, L.J.H. Bean, K. Stephens, A. Amemiya (Eds.), GeneReviews® [Internet]. Seattle (WA), University of Washington, Seattle, 1993-2019. Available from: https://www.ncbi.nlm.nih.gov/books/NBK1494/.

[7] F. Malfait, Vascular aspects of the Ehlers-Danlos Syndromes, Matrix Biol. 71-72 (2018) 380-395.

[8] T.K. Cooper, Q. Zhong, M. Krawczyk, H.J. Tae, G.A. Muller, R. Schubert, L.A. Myers, H.C. Dietz, M.I. Talan, W. Briest, The haploinsufficient *Col3a1* mouse as a model for vascular Ehlers-Danlos syndrome, Vet. Pathol. 47 (6) (2010) 1028-1039.

[9] S.W. Volk, Y. Wang, E.A. Mauldin, K.W. Liechty, S.L. Adams, Diminished type III collagen promotes myofibroblast differentiation and increases scar deposition in cutaneous wound healing, Cells Tissues Organs 194 (1) (2011) 25-37.

[10] R. Luo, S.J. Jeong, Z. Jin, N. Strokes, S. Li, X. Piao, G protein-coupled receptor 56 and collagen III, a receptor-ligand pair, regulates cortical development and lamination, Proc. Natl. Acad. Sci. U. S. A. 108 (31) (2011) 12925-12930.

[11] S.J. Jeong, S. Li, R. Luo, N. Strokes, X. Piao, Loss of *Col3a1*, the gene for Ehlers-Danlos syndrome type IV, results in neocortical dyslamination, PLoS One 7 (1) (2012) e29767.

[12] S.W. Volk, S.R. Shah, A.J. Cohen, Y. Wang, B.K. Brisson, L.K. Vogel, K.D. Hankenson, S.L. Adams, Type III collagen regulates osteoblastogenesis and the quantity of trabecular bone, Calcif. Tissue Int. 94 (6) (2014) 621-631.

[13] E.L. Miedel, B.K. Brisson, T. Hamilton, H. Gleason, G.P. Swain, L. Lopas, D. Dopkin, J.E. Perosky, K.M. Kozloff, K.D. Hankenson, S.W. Volk, Type III collagen modulates fracture callus bone formation and early remodeling, J. Orthop. Res. 33 (5) (2015) 675-684.

[14] B.K. Brisson, E.A. Mauldin, W. Lei, L.K. Vogel, A.M. Power, A. Lo, D. Dopkin, C. Khanna, R.G. Wells, E. Pure, S.W. Volk, Type III collagen directs stromal organization and limits metastasis in a murine model of breast cancer, Am. J. Pathol. 185 (5) (2015) 1471-1486.

[15] D.E. Birk, P. Brückner, Collagens, Suprastructures, and Collagen Fibril Assembly, in: R.P. Mecham (Ed.), The Extracellular Matrix: an Overview. Biology of Extracellular Matrix, Springer, Berlin, Heidelberg, 2011, pp. 77-115.

[16] R. Fleischmajer, E.D. MacDonald, J.S. Perlish, R.E. Burgeson, L.W. Fisher, Dermal collagen fibrils are hybrids of type I and type III collagen molecules, J. Struct. Biol. 105 (1-3) (1990) 162-169.

[17] S. D'Hondt, B. Guillemyn, D. Syx, S. Symoens, R. De Rycke, L. Vanhoutte, W. Toussaint, B.N. Lambrecht, A. De Paepe, D.R. Keene, Y. Ishikawa, H.P. Bachinger, S. Janssens, M.J.M. Bertrand, F. Malfait, Type III collagen affects dermal and vascular collagen fibrillogenesis and tissue integrity in a mutant *Col3a1* transgenic mouse model, Matrix Biol. 70 (2018) 72-83.

[18] R.D. Young, P.A. Lawrence, V.C. Duance, T. Aigner, P. Monaghan, Immunolocalization of collagen types II and III in single fibrils of human articular cartilage, J. Histochem. Cytochem. 48 (3) (2000) 423-432.
[19] J.J. Wu, M.A. Weis, L.S. Kim, D.R. Eyre, Type III collagen, a fibril network modifier in articular cartilage, J. Biol. Chem. 285 (24) (2010) 18537-18544.
[20] A.K. Williamson, A.C. Chen, R.L. Sah, Compressive properties and function-composition relationships of developing bovine articular cartilage, J. Orthop. Res. 19 (6) (2001) 1113-1121.
[21] V.C. Mow, S.C. Kuei, W.M. Lai, C.G. Armstrong, Biphasic creep and stress relaxation of articular cartilage in compression? Theory and experiments, J. Biomech. Eng. 102 (1) (1980) 73-84.
[22] H. Forster, J. Fisher, The influence of loading time and lubricant on the friction of articular cartilage, Proc. Inst. Mech. Eng. [H] 210 (2) (1996) 109-119.
[23] A. Maroudas, Physicochemical Properties of Articular Cartilage, in: M.A.R. Freeman (Ed.), Adult Articular Cartilage, Pitman, England, 1979, pp. 215-290.
[24] E.A. Makris, P. Hadidi, K.A. Athanasiou, The knee meniscus: structure-function, pathophysiology, current repair techniques, and prospects for regeneration, Biomaterials 32 (30) (2011) 7411-7431.
[25] D.L. Skaggs, W.H. Warden, V.C. Mow, Radial tie fibers influence the tensile properties of the bovine medial meniscus, J. Orthop. Res. 12 (2) (1994) 176-185.
[26] W. Petersen, B. Tillmann, Collagenous fibril texture of the human knee joint menisci, Anat. Embryol. 197 (4) (1998) 317-324.
[27] Q. Li, F. Qu, B. Han, C. Wang, H. Li, R.L. Mauck, L. Han, Micromechanical anisotropy and heterogeneity of the meniscus extracellular matrix, Acta Biomater. 54 (2017) 356-366.
[28] D. Eyre, Collagen of articular cartilage, Arthritis Res. 4 (1) (2002) 30-35.
[29] H.S. Cheung, Distribution of type I, II, III and V in the pepsin solubilized collagens in bovine menisci, Connect. Tissue Res. 16 (4) (1987) 343-356.
[30] S. Hosseininia, M.A. Weis, J. Rai, L. Kim, S. Funk, L.E. Dahlberg, D.R. Eyre, Evidence for enhanced collagen type III deposition focally in the territorial matrix of osteoarthritic hip articular cartilage, Osteoarthr. Cartilage 24 (6) (2016) 1029-1035.
[31] A.M. Teppo, T. Tornroth, E. Honkanen, C. Gronhagen-Riska, Urinary amino-terminal propeptide of type III procollagen (PIIINP) as a marker of interstitial fibrosis in renal transplant recipients, Transplantation 75 (12) (2003) 2113-2119.
[32] Y. Wang, Y. Li, A. Khabut, S. Chubinskaya, A.J. Grodzinsky, P. Önnerfjord, Quantitative proteomics analysis of cartilage response to mechanical injury and cytokine treatment, Matrix Biol. 63 (2017) 11-22.
[33] T. Mine, K. Ihara, H. Kawamura, R. Date, K. Umehara, Collagen expression in various degenerative meniscal changes: an immunohistological study, J. Orthop. Surg. 21 (2) (2013) 216-220.
[34] R.V. Iozzo, M.A. Gubbiotti, Extracellular matrix: the driving force of mammalian diseases, Matrix Biol. 71-72 (2018) 1-9.
[35] Y. Krishnan, A.J. Grodzinsky, Cartilage diseases, Matrix Biol. 71-72 (2018) 51-69.
[36] Q. Li, B. Doyran, L.W. Gamer, X.L. Lu, L. Qin, C. Ortiz, A.J. Grodzinsky, V. Rosen, L. Han, Biomechanical properties of murine meniscus surface via AFM-based nanoindentation, J. Biomech. 48 (8) (2015) 1364-1370.
[37] B. Doyran, W. Tong, Q. Li, H. Jia, X. Zhang, C. Chen, M. Enomoto-Iwamoto, X.L. Lu, L. Qin, L. Han, Nanoindentation modulus of murine cartilage: a sensitive indicator of the initiation and progression of post-traumatic osteoarthritis, Osteoarthr. Cartilage 25 (1) (2017) 108-117.
[38] B. Han, H.T. Nia, C. Wang, P. Chandrasekaran, Q. Li, D.R. Chery, H. Li, A.J. Grodzinsky, L. Han, AFM-nanomechanical test: an interdisciplinary tool that links the understanding of cartilage and meniscus biomechanics, osteoarthritis degeneration and tissue engineering, ACS Biomater. Sci. Eng. 3 (9) (2017) 2033-2049.
[39] B. Han, Q. Li, C. Wang, P. Patel, S.M. Adams, B. Doyran, H.T. Nia, R. Oftadeh, S. Zhou, C.Y. Li, X.S. Liu, X.L. Lu, M. Enomoto-Iwamoto, L. Qin, R.L. Mauck, R.V. Iozzo, D.E. Birk, L. Han, Decorin regulates the aggrecan network integrity and biomechanical functions of cartilage extracellular matrix, ACS Nano (2019) In press, doi: 10.1021/acsnano.1029b04477.

[40] F. Guilak, R.J. Nims, A. Dicks, C.L. Wu, I. Meulenbelt, Osteoarthritis as a disease of the cartilage pericellular matrix, Matrix Biol. 71-72 (2018) 40-50.
[41] W. Knudson, S. Ishizuka, K. Terabe, E.B. Askew, C.B. Knudson, The pericellular hyaluronan of articular chondrocytes, Matrix Biol. 78-79 (2019) 32-46.
[42] S.F. Wotton, V.C. Duance, Type III collagen in normal human articular cartilage, Histochem. J. 26 (5) (1994) 412-416.
[43] L. Han, A.J. Grodzinsky, C. Ortiz, Nanomechanics of the cartilage extracellular matrix, Annu. Rev. Mater. Res. 41 (2011) 133-168.
[44] T. Kawamoto, K. Kawamoto, Preparation of Thin Frozen Sections from Nonfixed and Undecalcified Hard Tissues Using Kawamot's Film Method (2012), in: M. Hilton (Ed.), Skeletal Development and Repair. Methods in Molecular Biology, Humana Press, Totowa, NJ, 2014, pp. 149-164.
[45] D.R. Chery, S.J. Rozans, B. Han, L. Qin, D.E. Birk, R.V. Iozzo, M. Enomoto-Iwamoto, L. Han, Direct investigation of the roles of decorin in cartilage pericellular matrix via immunofluorescence-guided AFM, Trans. Orthop. Res. Soc. 63 (2017) 165.
[46] C.A. Poole, S. Ayad, J.R. Schofield, Chondrons from articular cartilage: I. Immunolocalization of type VI collagen in the pericellular capsule of isolated canine tibial chondrons, J. Cell Sci. 90 (4) (1988) 635-643.
[47] S.R. Lamande, J.F. Bateman, Collagen VI disorders: insights on form and function in the extracellular matrix and beyond, Matrix Biol. 71-72 (2018) 348-367.
[48] R.E. Wilusz, L.E. DeFrate, F. Guilak, Immunofluorescence-guided atomic force microscopy to measure the micromechanical properties of the pericellular matrix of porcine articular cartilage, J. R. Soc. Interface 9 (76) (2012) 2997-3007.
[49] M.A. Batista, H.T. Nia, P. Önnerfjord, K.A. Cox, C. Ortiz, A.J. Grodzinsky, D. Heinegård, L. Han, Nanomechanical phenotype of chondroadherin-null murine articular cartilage, Matrix Biol. 38 (2014) 84-90.
[50] J.B. Freeman, R. Dale, Assessing bimodality to detect the presence of a dual cognitive process, Behav. Res. Methods 45 (1) (2013) 83-97.
[51] M. Yamauchi, M. Sricholpech, Lysine post-translational modifications of collagen, Essays Biochem. 52 (2012) 113-133.
[52] F.W. Roemer, M. Jarraya, J. Niu, J. Duryea, J.A. Lynch, A. Guermazi, Knee joint subchondral bone structure alterations in active athletes: a cross-sectional case-control study, Osteoarthr. Cartilage 23 (12) (2015) 2184-2190.
[53] D.F. Holmes, K.E. Kadler, The 10+4 microfibril structure of thin cartilage fibrils, Proc. Natl. Acad. Sci. U. S. A. 103 (46) (2006) 17249-17254.
[54] M.D. Buschmann, A.J. Grodzinsky, A molecular model of proteoglycan-associated electrostatic forces in cartilage mechanics, J. Biomech. Eng. 117 (2) (1995) 179-192.
[55] D. Dean, J. Seog, C. Ortiz, A.J. Grodzinsky, Molecular-level theoretical model for electrostatic interactions within polyelectrolyte brushes: applications to charged glycosaminoglycans, Langmuir 19 (13) (2003) 5526-5539.
[56] T.L. Vincent, C.J. McLean, L.E. Full, D. Peston, J. Saklatvala, FGF-2 is bound to perlecan in the pericellular matrix of articular cartilage, where it acts as a chondrocyte mechanotransducer, Osteoarthr. Cartilage 15 (7) (2007) 752-763.
[57] F. Guilak, A. Ratcliffe, V.C. Mow, Chondrocyte deformation and local tissue strain in articular cartilage: a confocal microscopy study, J. Orthop. Res. 13 (3) (1995) 410-421.
[58] J.B. Choi, I. Youn, L. Cao, H.A. Leddy, C.L. Gilchrist, L.A. Setton, F. Guilak, Zonal changes in the three-dimensional morphology of the chondron under compression: the relationship among cellular, pericellular, and extracellular deformation in articular cartilage, J. Biomech. 40 (12) (2007) 2596-2603.
[59] R. Madden, S.K. Han, W. Herzog, Chondrocyte deformation under extreme tissue strain in two regions of the rabbit knee joint, J. Biomech. 46 (3) (2013) 554-560.
[60] B.V. Nguyen, Q. Wang, N.J. Kuiper, A.J. El Haj, C.R. Thomas, Z. Zhang, Strain-dependent viscoelastic behaviour and rupture force of single chondrocytes and chondrons under compression, Biotechnol. Lett. 31 (6) (2009) 803-809.

[61] R.J. Wenstrup, J.B. Florer, E.W. Brunskill, S.M. Bell, I. Chervoneva, D.E. Birk, Type V collagen controls the initiation of collagen fibril assembly, J. Biol. Chem. 279 (51) (2004) 53331-53337.
[62] D. Heinegård, Proteoglycans and more – from molecules to biology, Int. J. Exp. Pathol. 90 (6) (2009) 575-586.
[63] D.E. Birk, F.H. Silver, Collagen fibrillogenesis in vitro: comparison of types I, II, and III, Arch. Biochem. Biophys. 235 (1) (1984) 178-185.
[64] R.C. Siegel, J.C. Fu, N. Uto, K. Horiuchi, D. Fujimoto, Collagen cross-linking: lysyl oxidase dependent synthesis of pyridinoline in vitro: confirmation that pyridinoline is derived from collagen, Biochem. Biophys. Res. Commun. 108 (4) (1982) 1546-1550.
[65] C.T. Hung, G.A. Ateshian, Grading of osteoarthritic cartilage: correlations between histology and biomechanics, J. Orthop. Res. 34 (1) (2016) 8-9.
[66] D.R. Eyre, M.A. Paz, P.M. Gallop, Cross-linking in collagen and elastin, Annu. Rev. Biochem. 53 (1984) 717-748.
[67] S. Kalamajski, C. Liu, V. Tillgren, K. Rubin, A. Oldberg, J. Rai, M. Weis, D.R. Eyre, Increased C-telopeptide cross-linking of tendon type I collagen in fibromodulin-deficient mice, J. Biol. Chem. 289 (27) (2014) 18873-18879.
[68] J.E. Marturano, J.D. Arena, Z.A. Schiller, I. Georgakoudi, C.K. Kuo, Characterization of mechanical and biochemical properties of developing embryonic tendon, Proc. Natl. Acad. Sci. U. S. A. 110 (16) (2013) 6370-6375.
[69] G.Y. Ng, B.W. Oakes, O.W. Deacon, I.D. McLean, D.R. Eyre, Long-term study of the biochemistry and biomechanics of anterior cruciate ligament-patellar tendon autografts in goats, J. Orthop. Res. 14 (6) (1996) 851-856.
[70] P. Hansen, B.T. Haraldsson, P. Aagaard, V. Kovanen, N.C. Avery, K. Qvortrup, J.O. Larsen, M. Krogsgaard, M. Kjaer, S. Peter Magnusson, Lower strength of the human posterior patellar tendon seems unrelated to mature collagen cross-linking and fibril morphology, J. Appl. Physiol. 108 (1) (2010) 47-52.
[71] S. Shalhub, J.H. Black, 3rd, A.C. Cecchi, Z. Xu, B.F. Griswold, H.J. Safi, D.M. Milewicz, N.B. McDonnell, Molecular diagnosis in vascular Ehlers-Danlos syndrome predicts pattern of arterial involvement and outcomes, J. Vasc. Surg. 60 (1) (2014) 160-169.
[72] P. Panwar, G.S. Butler, A. Jamroz, P. Azizi, C.M. Overall, D. Bromme, Aging-associated modifications of collagen affect its degradation by matrix metalloproteinases, Matrix Biol. 65 (2018) 30-44.
[73] M. Nomura, N. Sakitani, H. Iwasawa, Y. Kohara, S. Takano, Y. Wakimoto, H. Kuroki, H. Moriyama, Thinning of articular cartilage after joint unloading or immobilization. An experimental investigation of the pathogenesis in mice, Osteoarthr. Cartilage 25 (5) (2017) 727-736.
[74] R.W. Farndale, D.J. Buttle, A.J. Barrett, Improved quantitation and discrimination of sulphated glycosaminoglycans by use of dimethylmethylene blue, Biochim. Biophys. Acta. 883 (2) (1986) 173-177.
[75] M.D. Buschmann, Y.J. Kim, M. Wong, E. Frank, E.B. Hunziker, A.J. Grodzinsky, Stimulation of aggrecan synthesis in cartilage explants by cyclic loading is localized to regions of high interstitial fluid flow, Arch. Biochem. Biophys. 366 (1) (1999) 1-7.
[76] M.A. Sweigart, C.F. Zhu, D.M. Burt, P.D. DeHoll, C.M. Agrawal, T.O. Clanton, K.A. Athanasiou, Intraspecies and interspecies comparison of the compressive properties of the medial meniscus, Ann. Biomed. Eng. 32 (11) (2004) 1569-1579.
[77] H.T. Nia, S.J. Gauci, M. Azadi, H.H. Hung, E. Frank, A.J. Fosang, C. Ortiz, A.J. Grodzinsky, High-bandwidth AFM-based rheology is a sensitive indicator of early cartilage aggrecan degradation relevant to mouse models of osteoarthritis, J. Biomech. 48 (1) (2015) 162-165.
[78] E.K. Dimitriadis, F. Horkay, J. Maresca, B. Kachar, R.S. Chadwick, Determination of elastic moduli of thin layers of soft material using the atomic force microscope, Biophys. J. 82 (5) (2002) 2798-2810.
[79] D.F. Bray, J. Bagu, P. Koegler, Comparison of hexamethyldisilazane (HMDS), Peldri II, and critical-point drying methods for scanning electron microscopy of biological specimens, Microsc. Res. Tech. 26 (6) (1993) 489-495.

[80] H.L. Ansorge, X. Meng, G. Zhang, G. Veit, M. Sun, J.F. Klement, D.P. Beason, L.J. Soslowsky, M. Koch, D.E. Birk, Type XIV collagen regulates fibrillogenesis: premature collagen fibril growth and tissue dysfunction in null mice, J. Biol. Chem. 284 (13) (2009) 8427-8438.
[81] M. Yamauchi, Y. Taga, S. Hattori, M. Shiiba, M. Terajima, Analysis of collagen and elastin cross-links, Methods Cell Biol. 143 (2018) 115-132.
[82] M. Terajima, Y. Taga, W.A. Cabral, M. Nagasawa, N. Sumida, S. Hattori, J.C. Marini, M. Yamauchi, Cyclophilin B deficiency causes abnormal dentin collagen matrix, J. Proteome Res. 16 (8) (2017) 2914-2923.
[83] H. Huang, J.D. Skelly, D.C. Ayers, J. Song, Age-dependent changes in the articular cartilage and subchondral bone of C57BL/6 mice after surgical destabilization of medial meniscus, Sci. Rep. 7 (2017) 42294.
[84] Y.H. Sniekers, F. Intema, F.P. Lafeber, G.J. van Osch, J.P. van Leeuwen, H. Weinans, S.C. Mastbergen, A role for subchondral bone changes in the process of osteoarthritis; a micro-CT study of two canine models, BMC Musculoskelet. Disord. 9 (2008) 20.

FIGURE LEGENDS

Figure 1 Distribution of collagen III in articular cartilage and the impact of collagen III on cartilage gross-level morphology. a) Quantitative PCR (qPCR) showed that in *Col3a1*$^{+/-}$ (+/–) mouse, the expression of *Col3a1* gene was significantly reduced by ≈ 50% in both articular cartilage and meniscus ($n = 4$ for wild-type (+/+), $n = 3$ for +/–, mean ± SEM, $p < 0.01$), while other major matrix genes were not significantly affected (*Col2a1*, *Acan* in articular cartilage and *Col1a1*, *Col2a1* in meniscus). b) Immunohistochemistry (IHC) of collagen III in murine articular cartilage did not show clear distribution pattern of collagen III at 2-week age, but detected intense localization in the PCM at 2-month age, and reduced staining in *Col3a1*$^{+/-}$ cartilage. Shown together is the negative internal control of WT cartilage stained without primary antibody. c) Western blot on recombinant human collagen I, III and collagen II extracted from human articular cartilage validated the specificity of the antibody for collagen III, AB7778. d) Safranin-O/Fast Green histology illustrated no appreciable differences in the staining of sGAGs or joint morphology between +/+ and +/– mouse knee articular cartilage at both 2-week and 2-month ages. e) No significant differences were found in the thicknesses of uncalcified or total cartilage and the amount of sGAGs between 2-month-old +/+ and +/– cartilage (mean ± 95% CI, $n \geq 6$ for each genotype).

Figure 2 Impact of collagen III reduction on the whole tissue modulus of a) articular cartilage and b) meniscus, as measured by AFM-nanoindentation using microspherical tips ($R \approx 5$ μm) in PBS (mean ± 95% CI, $n \geq 5$). Each data point represented the average modulus of ≥ 10 indentation locations from one animal. Different letters indicated significant age-dependent differences within the same genotype, $p < 0.05$. *: $p < 0.01$ between untreated and chondroitinase ABC (C'ABC)-treated groups within the same genotype at 2-month age.

Figure 3 Impact of collagen III reduction on the micromechanical properties of articular cartilage PCM and T/IT-ECM. a) Representative collagen VI IF images of 2-month-old wild-type (+/+) and *Col3a1*$^{+/-}$ (+/–) tibia cartilage sagittal sections. b) Box-and-whisker plots of the distribution of cartilage PCM thickness (≥ 120 cells from $n = 6$ animals for each genotype, p-value was obtained via unpaired two-sample student's t-test on the PCM thickness values pooled from the six animals). c) Schematics of collagen VI IF-guided AFM-nanoindentation mapping experimental set-up and representative map of indentation modulus, E_{ind}, from 2-month-old WT cartilage, which illustrated the separation of the PCM and T/IT-ECM microdomains. d) Box-and-whisker plot of E_{ind} distribution on the PCM (≥ 600 locations from $n = 6$ animals for each genotype) and T/IT-ECM (≥ 2,800 locations, $n = 6$, p-values were obtained via Mann-Whitney test on the averaged modulus from each animal). Panels b, d: Each data point represents the average value measured from one animal.

Figure 4 Impact of collagen III reduction on the nanostructure of collagen fibrils on the surfaces of articular cartilage and meniscus. a) Representative SEM images of collagen fibril structure on the surfaces of 2-month-old wild-type (+/+) and *Col3a1*$^{+/-}$ (+/–) cartilage and meniscus. b) Box-and-whisker plot of fibril diameter distributions (≥ 200 fibrils from $n = 4$ animals for each genotype and tissue type at each age).

Figure 5 Impact of collagen III reduction on the nanostructure of collagen fibrils in the PCM and T/IT-ECM of articular cartilage. a) Representative TEM images of collagen fibril structure on the sagittal sections of 2-month-old wild-type (+/+) and *Col3a1*$^{+/-}$ (+/–) cartilage PCM and T/IT-ECM. b) Histogram of fibril diameter distribution (> 130 fibrils from $n = 4$ animals for each genotype in each region). Shown together were the normal distribution, $N(\mu, \sigma^2)$, fits to fibril diameters (for each fit, values of μ and σ correspond to the mean and standard deviation of fibril diameters shown in Table 2). c) Comparison of fibril diameter heterogeneity (variance) between the two genotypes (mean ± 95% CI, > 130 fibrils, $n = 4$).

Figure 6 Impact of collagen III reduction on the nanostructure of collagen fibrils in the ECM of the meniscus tissue interior. a) Representative TEM images of collagen fibril structure on the sagittal sections of 2-month-old wild-type (+/+) and *Col3a1*$^{+/-}$ (+/–) meniscus ECM. b) Histogram of fibril diameter distribution (> 600 fibrils from $n = 4$ animals for each genotype). Shown together were the normal distribution fits to fibril diameters,

unimodal for +/+ ($N(\mu, \sigma^2)$, $\mu = 72.6$, $\sigma = 28.3$) and bimodal for +/– ($p \cdot N(\mu_1, \sigma_1^2) + (1 - p) \cdot N(\mu_2, \sigma_2^2)$, $p = 0.87$, $\mu_1 = 69.2$, $\sigma_1 = 23.8$, $\mu_2 = 158.3$, $\sigma_2 = 29.5$). c,d) Comparisons of c) fibril diameter heterogeneity (variance) and d) fibril packing density between the two genotypes (mean ± 95% CI, calculated from > 600 fibrils in ≥ 16 ROIs, $n = 4$ animals).

Figure 7 Impact of collagen III reduction on the covalent cross-linking in the collagen fibrils of articular cartilage (AC) and meniscus (M). a,b) Comparisons of collagen amount and cross-linking between wild-type (+/+) and *Col3a1*$^{+/-}$ (+/–) tissues, a) total collagen amount, and b) cross-linking analysis of the immature cross-link dihydroxylysinonorleucine (DHLNL), mature cross-link pyrodinoline (Pyd) and deoxy-pyrodinoline (de-Pyd) and total LOX-mediated aldehyde densities. c) Western blot on the expression of LOX and associated semi-quantitative levels of LOX content, as normalized to the internal GAPDH control. All the results were obtained from 2-month-old tissues (mean ± SD, $n = 4$ biological repeats for articular cartilage, and $n = 3$ for meniscus). Each data point represents one biological repeat measured from tissues pooled from 3 animals.

Figure 8 Impact of collagen III reduction on the subchondral bone structure. a) Representative frontal plane of µCT image (L: lateral, M: medial). b,c) Comparison of subchondral bone structural parameters between 2-month-old wild-type (+/+) and *Col3a1*$^{+/-}$ (+/–) mice, including b) Subchondral bone plate thickness (SBP Th.), and c) Subchondral trabecular bone (STB) structural characteristics, including bone volume fraction (BV/TV), trabecular number (Tb.N), trabecular thickness (Tb.Th) and trabecular separation (Tb.Sp). No significant difference was detected between the two genotypes (mean ± SD, $n = 5$). Each data point represents the average value measured from one animal.

Figure 9 Schematic illustration of the working hypothesis on the structural role of collagen III in articular cartilage ECM, inspired by [19, 40, 62]. a) Upper panel: Collagen III co-assembles with collagen II on fibrillar surfaces during the initial phase of collagen fibrillogenesis in the PCM, and forms covalent cross-links with collagen II and other collagen III molecules. The un-processed N-propeptide limits the lateral growth of collagen II fibrils (collagens IX and XI are not shown to increase clarity). Lower panel: The PCM has distinctive structure and composition in comparison to the further-removed T/IT-ECM, as characterized by the localization of collagen VI, perlecan and biglycan. In the PCM, collagen III could play a role in regulating the initial stage of collagen II fibrillogenesis. b) Reduction of collagen III increases the fibril diameter and heterogeneity in cartilage matrix, and alters the covalent cross-linking patterns of the fibrillar network. This could potentially alter the molecular conformation of aggrecan aggregates. In the schematics, the packing densities of collagen fibrils and aggrecan networks are reduced to increase clarity.

TABLES

Table 1 Summary of collagen fibril diameter distributions on the surface of articular cartilage and meniscus, measured by scanning electron microscopy (SEM)

unit (nm)	Articular Cartilage				Meniscus	
	2-week		2-month		2-month	
	+/+	+/–	+/+	+/–	+/+	+/–
mean	21	22	23	27	33	36
std	5	5	7	9	17	18
Q_1	18	19	19	21	22	25
Q_2	20	21	22	25	27	31
Q_3	24	24	27	31	36	40
min	9	8	12	9	12	12
max	41	40	63	54	115	121
n_{fibrils}	300	300	210	210	290	442

Table 2 Summary of collagen fibril diameter distributions in the matrix interior of 2-month-old articular cartilage and meniscus, measured by transmission electron microscopy (TEM)

unit (nm)	Articular Cartilage				Meniscus	
	PCM		T/IT-ECM		ECM	
	+/+	+/–	+/+	+/–	+/+	+/–
mean	35	53	47	55	73	81
std	8	16	13	18	28	39
Q_1	30	43	38	44	51	53
Q_2	35	51	45	53	71	74
Q_3	40	60	56	64	93	97
min	18	25	16	18	13	18
max	69	107	83	113	148	220
n_{fibrils}	235	137	228	217	821	624

Table 3 List of primers used for quantitative RT-PCR

Gene	Forward Primer	Reverse Primer
Col1a1	5'-TTCTCCTGGCAAAGACGGACTCAA-3'	5'-AGGAAGCTGAAGTCATAACCGCCA-3'
Col2a1	5'-GCTGGTGCACAAGGTCCTAT-3'	5'-ACCCTGCAGTCCAGTGAAAC-3'
Col3a1	5'-TGGTCCTCAGGGTGTAAAGG-3'	5'-GTCCAGCATCACCTTTTG GT-3'
Acan	5'-GACTGTGTGGTGATGATCTG-3'	5'-CTCGTAGCGATCTTTCTTCTG-3'
β-actin	5'-AGATGACCCAGATCATGTTTGAGA-3'	5'-CACAGCCTGGATGGCTACGT-3'
Gapdh	5'- TCAACAGCAACTCCCACTCTTCCA-3'	5'-ACCCTGTTGCTGTAGCCGTATTCA-3'

Figure 1

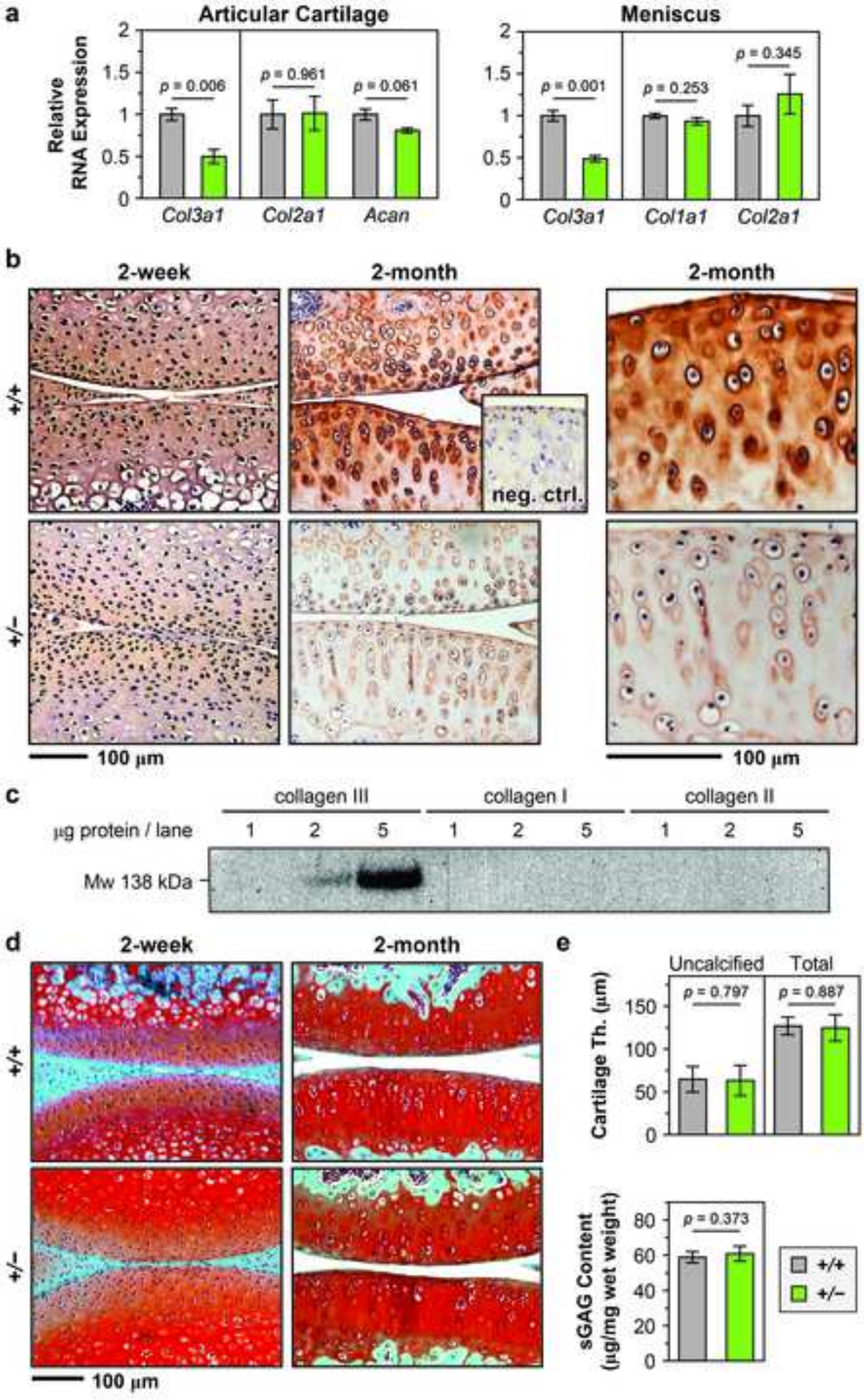

Figure 2

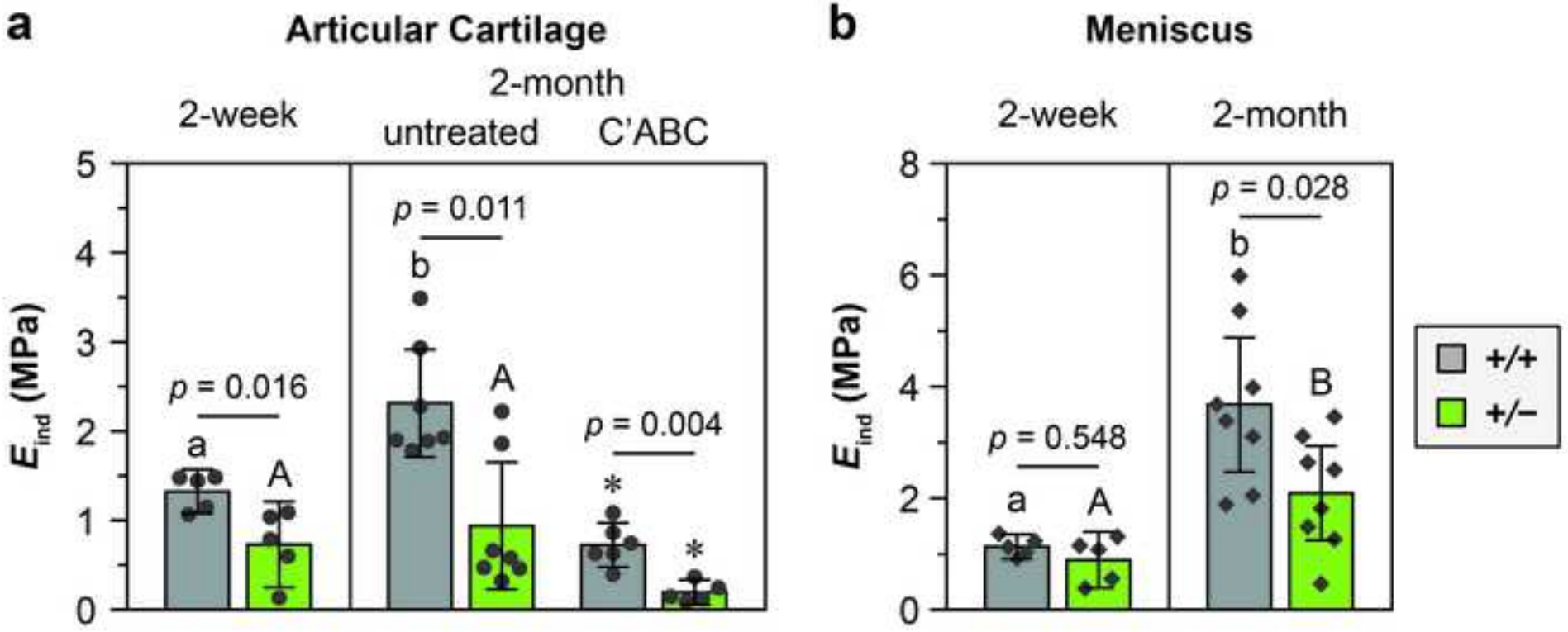

Figure 3

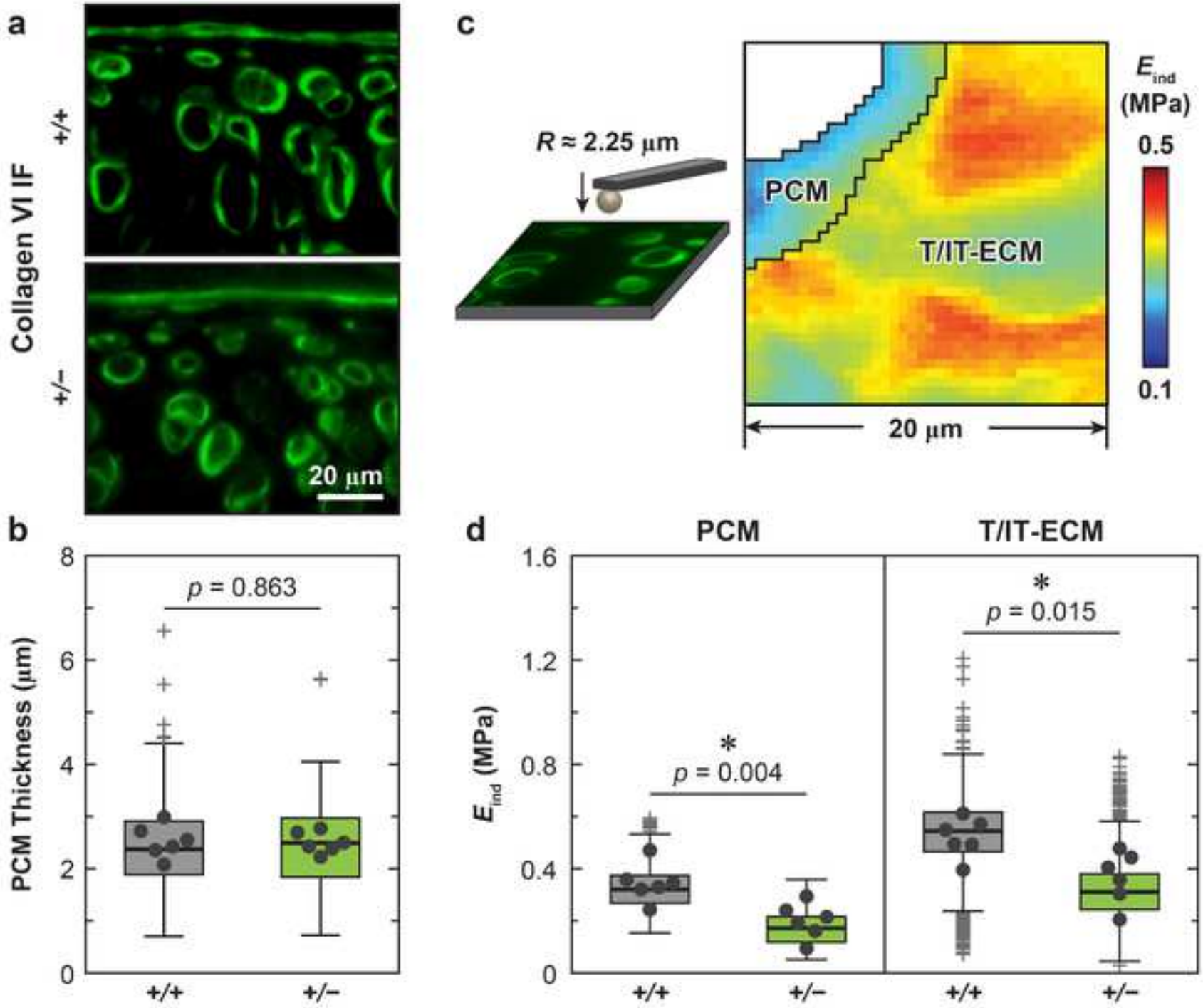

Figure 4

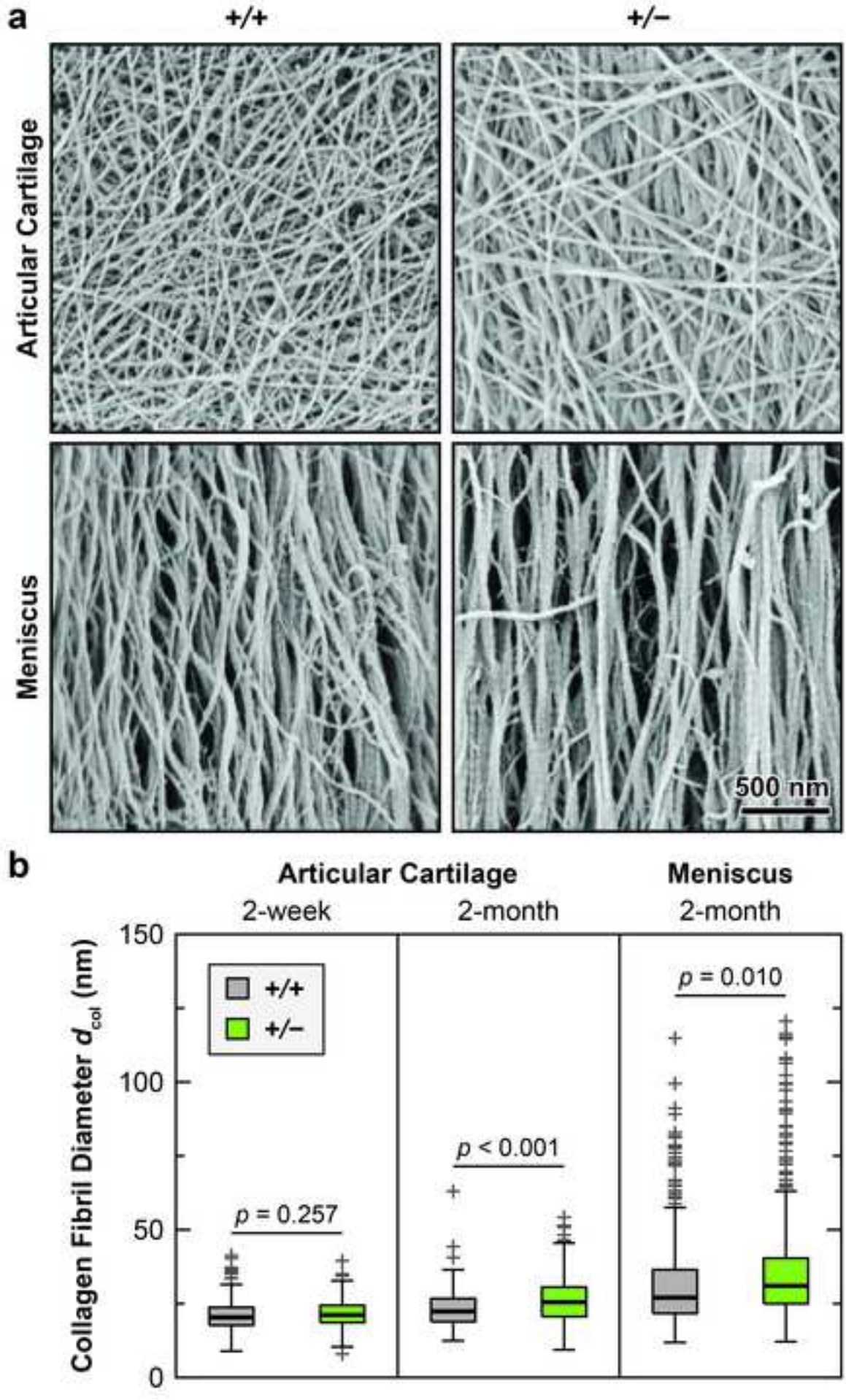

Figure 5

Click here to access/download;Figure;Fig 5_TEM_Cartilage-01.tif

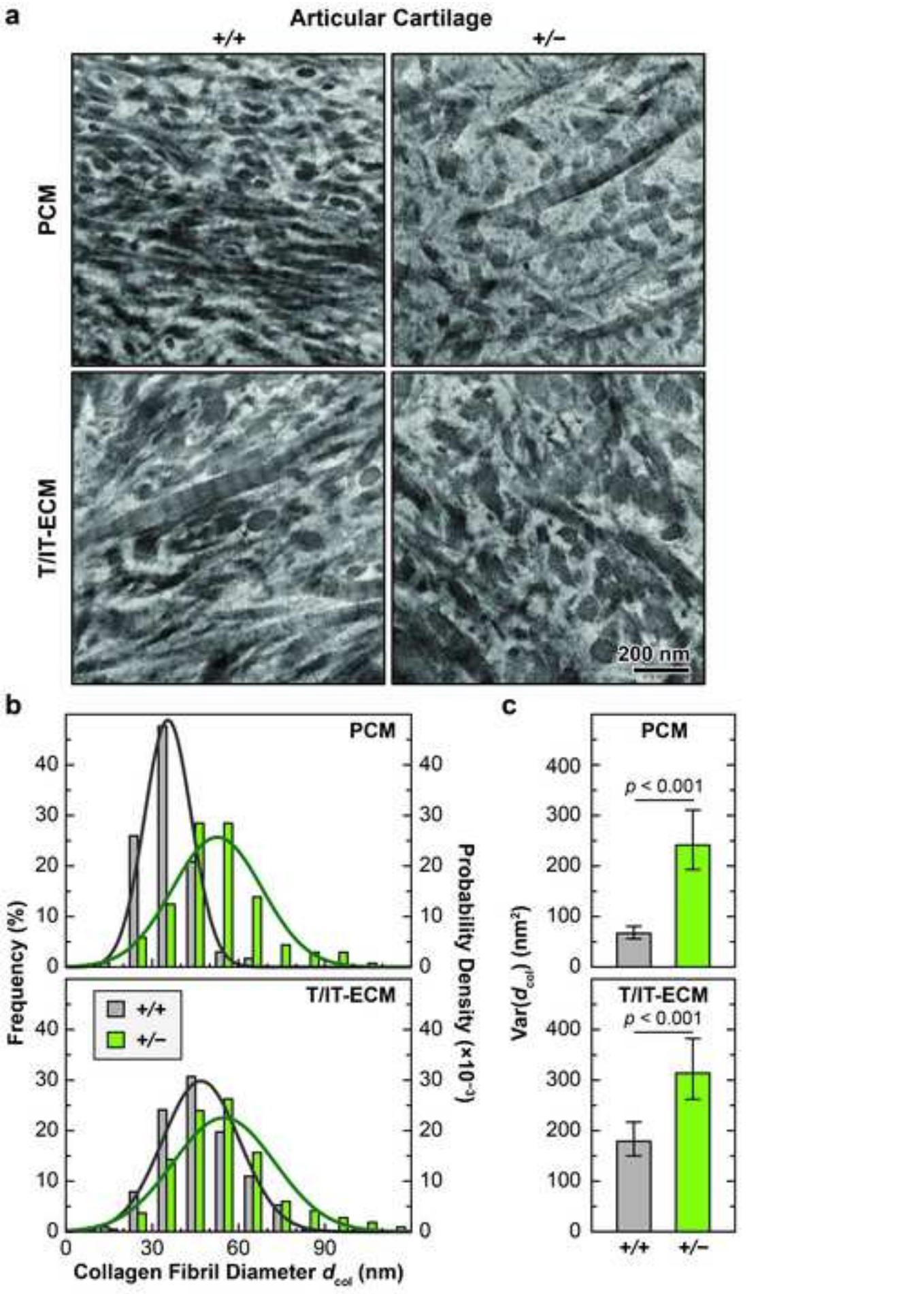

Figure 6

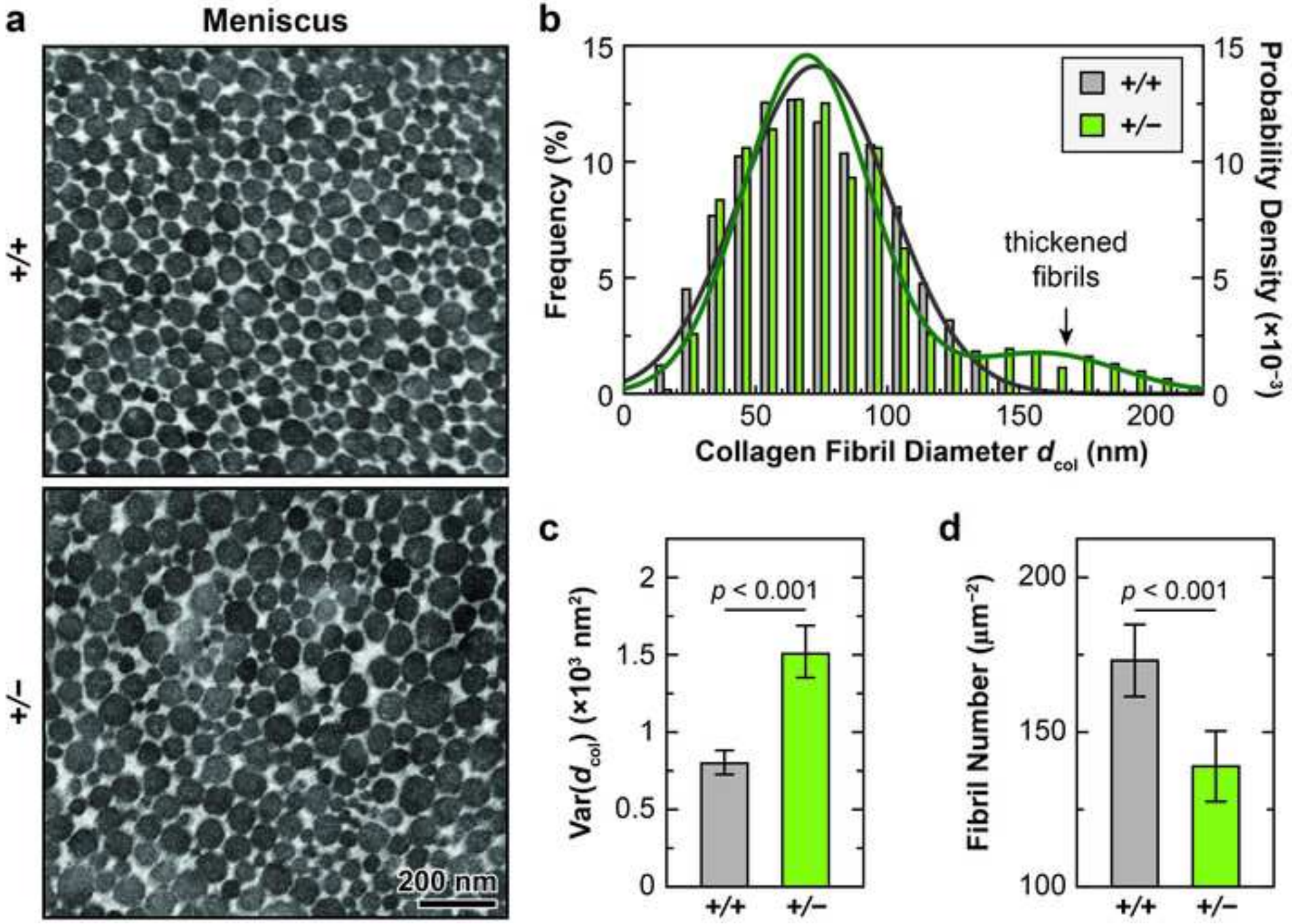

Figure 7

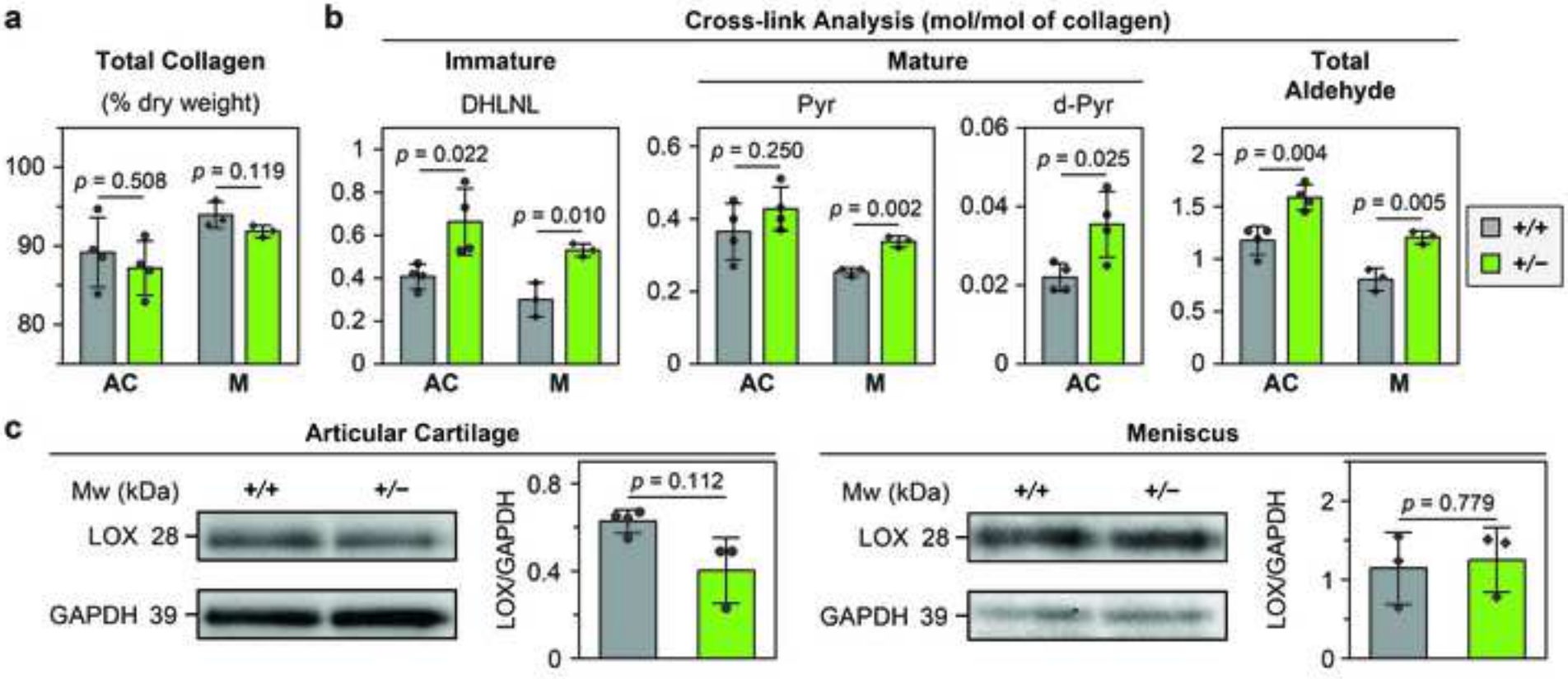

Figure 8

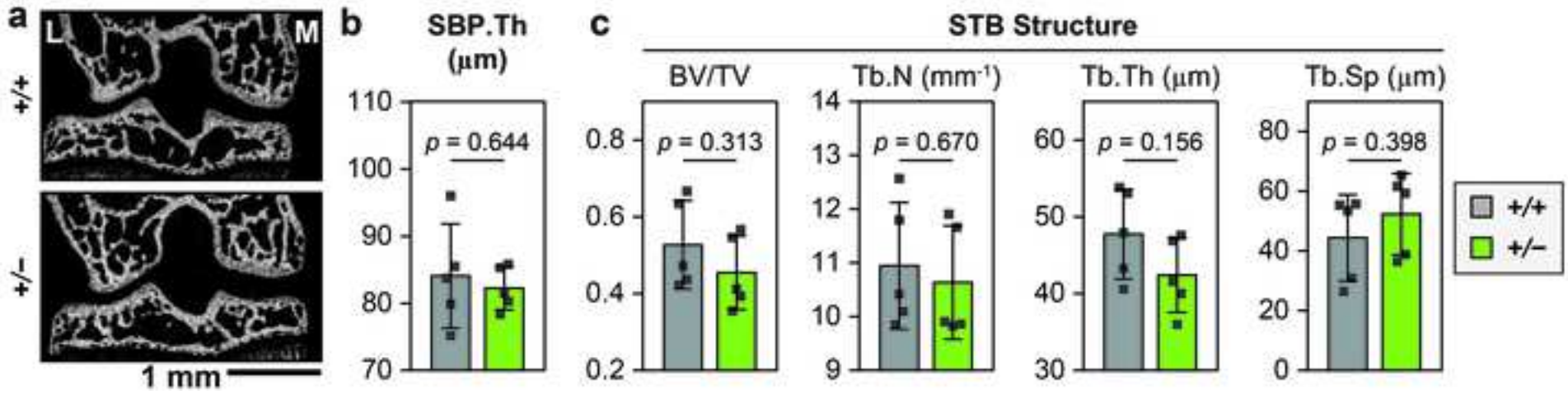

Figure 9

Click here to access/download;Figure;Fig 9_Schematic-01.tif